NASA CONTRACTOR REPORT

NASA CR-1315

NUCLEAR STUDIES OF THE NUCLEAR LIGHT BULB ROCKET ENGINE

by Thomas S. Latham

Prepared by
UNITED AIRCRAFT CORPORATION
East Hartford, Conn.
for

NATIONAL AERONAUTICS AND SPACE ADMINISTRATION • WASHINGTON, D. C. • APRIL 1969

NASA CR-1315

NUCLEAR STUDIES OF THE NUCLEAR LIGHT BULB ROCKET ENGINE

By Thomas S. Latham

Issued by Originator as Report No. G-910375-3

Prepared under Contract No. NASw-847 by
UNITED AIRCRAFT CORPORATION
East Hartford, Conn.

for

NATIONAL AERONAUTICS AND SPACE ADMINISTRATION

For sale by the Clearinghouse for Federal Scientific and Technical Information
Springfield, Virginia 22151 – CFSTI price $3.00

FOREWORD

An exploratory experimental and theoretical investigation of gaseous nuclear rocket technology is being conducted by the United Aircraft Research Laboratories under Contract NASw-847 with the joint AEC-NASA Space Nuclear Propulsion Office. The Technical Supervisor of the Contract for NASA is Captain C. E. Franklin (USAF). Results of portions of the investigation conducted during the period between September 15, 1967 and September 15, 1968 are described in the following five reports (including the present report) which comprise the required eighth Interim Summary Technical Report under the Contract:

1. Kendall, J. S., W. C. Roman, and P. G. Vogt: Initial Radio-Frequency Gas Heating Experiments to Simulate the Thermal Environment in a Nuclear Light Bulb Reactor. United Aircraft Research Laboratories Report G-910091-17, September 1968.

2. Mensing, A. E. and L. R. Boedeker: Theoretical Investigation of R-F Induction Heated Plasmas. United Aircraft Research Laboratories Report G-910091-18, September 1968.

3. Krascella, N. L.: Theoretical Investigation of the Composition and Line Emission Characteristics of Argon-Tungsten and Argon-Uranium Plasmas. United Aircraft Research Laboratories Report G-910092-10, September 1968.

4. Marteney, P. J., A. E. Mensing, and N. L. Krascella: Experimental Investigation of the Spectral Emission Characteristics of Argon-Tungsten and Argon-Uranium Induction Heated Plasmas. United Aircraft Research Laboratories Report G-910092-11, September 1968.

5. Latham, T. S.: Nuclear Studies of the Nuclear Light Bulb Rocket Engine. United Aircraft Research Laboratories Report G-910375-3, September 1968. (present report)

Nuclear Studies of the Nuclear Light Bulb Rocket Engine

TABLE OF CONTENTS

TABLE OF CONTENTS (Continued)

Nuclear Studies of the Nuclear Light Bulb Rocket Engine

SUMMARY

Analytical studies were conducted to determine U-233 critical mass requirements, neutron kinetic behavior, and neutron and gamma ray heating rates for the nuclear light bulb rocket engine. The nuclear light bulb is a multiple-cavity gaseous nuclear rocket engine in which energy is transferred by thermal radiation from gaseous nuclear fuel through internally cooled transparent walls to seeded hydrogen propellant. The engine considered in this report employs seven separate cavities, each having a length of 6 ft and an average diameter of 2.3 ft. Beryllium oxide is employed between the unit cavities, and layers of BeO and graphite surround the seven units to provide neutron reflection.

The criticality analysis allowed the effects of engine design changes on critical mass to be investigated. Among the factors that were varied were the total moderator mass, the amount of BeO between unit cavities, the distribution of moderator mass, the amount of tungsten seed in the hydrogen propellant, and the amount of hafnium required to shield the fuel injection and recirculation system ducts. The analysis also considered factors affecting the kinetic behavior of a nuclear light bulb engine. The effects of variations in fuel region radius, mixed-mean propellant temperature, nominal system operating temperature, system operating pressure, and the proportion by weight of tungsten seed in the hydrogen propellant were investigated. For one specific nuclear light bulb engine configuration, prompt neutron lifetime was calculated, and comparisons of critical masses were made for U-233, U-235, and Pu-239.

Neutron kinetic equations were formulated which allowed for variable loss rates of both nuclear fuel and delayed neutron precursors. Power level responses to step, ramp, and oscillatory variations in both reactivity and fuel loss rate were obtained.

Neutron and gamma ray heating rates were calculated for a specific nuclear light bulb engine to provide information on requirements for cooling engine components and the location and design of heat exchangers. Radiation dose rates in the transparent wall materials were calculated and compared with the dose rates of various test reactors. Dosages in the filament-wound fiberglas pressure vessel were also calculated to evaluate the potential for degradation of pressure vessel strength due to radiation damage.

MAJOR RESULTS

1. The total critical uranium-233 mass for all seven units of the reference engine employed in the study was determined to be 34.7 lb on the basis of two-dimensional neutron diffusion theory and 30.9 lb on the basis of two-dimensional neutron transport theory. These values of critical mass correspond to average fuel partial pressures in the fuel-containment region of 200 and 175 atm, respectively, for an average fuel temperature of 42,000 R and a fuel-region volume of 34% of the cavity volume.

2. Power doubling times of from 1 to 20 sec were calculated for representative step and ramp changes in reactivity and fuel decay constant. However, the control problem has not yet been analyzed to determine if some control other than that of fuel flow will be required to maintain constant engine power.

3. The distribution of power deposited in various components for a total engine power of 4600 megw and an average fuel residence time of 20 sec was calculated to be as follows: fuel region, 4131.6 megw; moderator region, 210.6 megw; heat exchanger region, 144 megw; hot gas region between fuel and cavity walls, 74.9 megw (including 58.7 megw in the hydrogen propellant); pressure shell, 17.4 megw; and leakage out of reactor, 21.5 megw.

DETAILED RESULTS

Criticality Calculations

1. The following results were determined on the basis of two-dimensional neutron diffusion theory calculations:

   a. A U-233 critical mass of 34.7 lb was determined for the reference engine, corresponding to an average fuel partial pressure in the fuel-containment region of 200 atm.

   b. The optimum fraction of radial moderator to total moderator mass (the ratio of moderator mass surrounding the unit cavities to the total moderator mass surrounding the cavities and in the end walls) was found to be 0.5; this resulted in minimum critical mass for the reference engine.

   c. The U-233 critical mass increased essentially linearly with increase in effective nozzle throat area for the reference engine. The ratio of fractional fuel mass change to fractional change in effective nozzle throat area was $(\Delta M/M_C)/(\Delta A_T/A_{T_\odot}) = +0.156$.

   d. Inclusion of tungsten seed at 4% by weight in the hydrogen propellant increased critical mass by only 0.09 lb.

   e. Reduction of hafnium in the upper end walls by a factor of one-half decreased critical mass by only 0.36 lb.

   f. A positive reactivity coefficient resulted from an increase in nominal operating pressure.

   g. A small negative reactivity coefficient resulted from an increase in the amount of tungsten seed in the hydrogen propellant.

   h. Prompt neutron lifetime for the reference engine was calculated to be 0.516 msec.

2. The following results were determined on the basis of one-dimensional neutron transport theory calculations:

   a. The optimum internal moderation fraction for the reference engine was 0.19, but due to considerations of flattening power density, an internal moderation fraction of 0.14 was chosen for the reference engine.

b. Positive reactivity coefficients resulted from increases in nominal operating temperature and mixed-mean propellant temperature.

c. A negative reactivity coefficient resulted from an increase in fuel radius when the fuel cloud radius was changed while chamber pressure and U-233 mass remained constant.

d. Critical masses using U-235 and Pu-239 in the reference engine were 50.4 and 46.0 lb, respectively, compared with 34.7 lb for U-233.

3. The following result was determined on the basis of two-dimensional neutron transport theory calculations:

a. A U-233 critical mass of 30.9 lb was determined for the reference engine, which is 11.0% less than that calculated using two-dimensional diffusion theory. This compares to a U-233 critical mass of 43.5 lb for an earlier reference engine with substantially greater amounts of neutron-absorbing structural materials in the end walls and nozzle approach regions. The critical mass of 30.9 lb corresponds to an average fuel partial pressure of 175 atm in the fuel-containment region.

Nuclear Kinetics Studies

1. Step and ramp variations in reactivity and fuel decay constant (the inverse of average fuel residence time) were studied using the neutron kinetic equations with the following responses in engine power level:

a. For an average fuel residence time of 20.0 sec (fuel decay constant of 0.05 sec^{-1}) and a prompt neutron lifetime of 5×10^{-4} sec, power level doubling times for step and ramp insertions of reactivity of 0.20β and $0.20\beta\,(t-t_o)$ and for step and ramp changes of fuel decay constant of $-0.01\lambda_{F_o}$ and $-0.01\,\lambda_{F_o}\,(t-t_o)$ sec^{-1} were of the order of 2.0 to 4.0 sec.

b. The effect of changing fuel decay constant to 0.0 sec^{-1} (infinite average fuel residence time) was to increase power level doubling time for the step and ramp insertions of reactivity used in (a) above to the order of 15.0 to 20.0 sec.

c. Variations in prompt neutron lifetime from 10^{-4} to 3×10^{-3} sec (more than an order of magnitude) caused increases in power level doubling times by factors of 2.0 to 3.0 for the step and ramp variations in reactivity and fuel decay constant used in (a).

d. Variations in the initial value of fuel decay constant from 0.02 to 1.0 sec^{-1} caused a decrease in power level doubling times by a factor of about 5.0 for the ramp variations in fuel decay constant used in (a).

2. Oscillatory variations in reactivity and fuel decay constant were studied using the neutron kinetic equations with the following responses in neutron level:

a. The gain in decibels in the amplitude of neutron level oscillations relative to the amplitude of oscillations in reactivity, $20 \log_{10}\left[(\Delta n/n_o)/(\delta k/k)\right]$, was about 83 db for frequencies below 3 rad/sec and decreased at a rate of 20 db/decade for frequencies above about 3 rad/sec. Fuel decay constant was 0.05 sec^{-1} and prompt neutron lifetime was 5×10^{-4} sec for these cases.

b. The gain in decibels in the amplitude of neutron level oscillations relative to the amplitude of oscillations in fuel decay constant, $20 \log_{10}\left[(\Delta n/n_o)/(\delta \lambda_F/\lambda_{F_o})\right]$, was about 32 db at 0.3 rad/sec, decreased at a rate of 40 db/decade for frequencies above 3 rad/sec. Fuel decay constant was 0.05 sec^{-1} and prompt neutron lifetime was 5×10^{-4} sec for these cases.

c. The phase difference between neutron level oscillations and reactivity oscillations reached a minimum of -30 deg at about 0.5 rad/sec and approached an asymptotic value of -90 deg above 50 rad/sec. The phase difference between neutron level oscillations and fuel decay constant oscillations was about -110 deg at frequencies below 0.3 rad/sec and approached an asymptotic value of -180 deg above 50 rad/sec. The latter 180 deg phase difference is not expected to cause instabilities because gain is of the order of -40 db at 50 rad/sec. Fuel decay constant was 0.05 sec^{-1} and prompt neutron lifetime was 5×10^{-4} sec for these cases.

d. The principal effect of changing the value of initial fuel decay constant from 0.05 to 0.5 sec^{-1} was to increase gain in neutron flux level response to both reactivity and fuel decay constant oscillations by about 20 db over all frequencies.

Neutron and Gamma Ray Heating

1. The following results were determined on the basis of detailed neutron and gamma ray heating calculations:

a. The fission fragment and beta energy release rates in the fuel regions were estimated to be 4036, 4131.6, and 4147.6 megw while the neutron and gamma ray energy release rates in the active core were estimated to be 296, 325, and 342 megw for average fuel residence times of 1.0, 20, and 60 sec, respectively. Correspondingly, the rate of energy release from delayed beta particles and gamma rays in the fuel separation and recirculation system was estimated to be 268, 143, and 110 megw for average fuel residence times of 1.0, 20, and 60 sec, respectively. For purposes of this study, it was assumed that all of the energy released in the fuel separation and recirculation system was absorbed by the heavy metals in the turbine, pumps, plumbing, heat exchangers, and support structure in the upper dome of the pressure vessel.

b. The distribution of power deposited in various components for a total engine power of 4600 megw and an average fuel residence time of 20 sec was calculated to be as follows: fuel region, 4131.6 megw; moderator region, 210.6 megw; heat exchanger region, 144 megw; hot gas region between fuel and cavity walls, 74.9 megw (including 58.7 megw in the hydrogen propellant); pressure shell, 17.4 megw; and leakage out of reactor, 21.5 megw.

c. Direct heating of hydrogen propellant located between the fuel regions and cavity walls by neutron energy degradation was calculated to be 54.3 megw.

d. The rate of energy leakage from the entire system was calculated to be 6.2 megw for neutrons and 13.2, 15.3, and 16.6 megw for gamma rays for average fuel residence times of 1.0, 20, and 60 sec, respectively.

e. The average dose rate in the filament-wound fiberglas pressure vessel was calculated to be 0.17 mrad/sec. This would allow about six full-power runs of 1000-sec duration before the total dose became 1000 mrad, the estimated allowable dosage before degradation of the laminate strength commences. However, hot spots, particularly in the lower pressure vessel, with dose rates as high as 3.69 mrad/sec were calculated. This indicates a need for further investigation and the possible inclusion of a heat shield across the inner wall of the lower pressure vessel.

f. Secondary sources due to thermal neutron capture, (n, γ) reactions, in the pressure vessel contribute a gamma source equal to about 16.5 percent of the energy deposition rate in the pressure vessel due to fission neutrons and gamma rays. In all other regions, secondary source strengths amount to less than 5 percent of the total energy deposition rate.

INTRODUCTION

An experimental and theoretical investigation of gaseous nuclear rocket technology is being conducted by the United Aircraft Research Laboratories under Contract NASw-847 administered by the joint AEC-NASA Space Nuclear Propulsion Office. These investigations are directed primarily toward determining the feasibility of the closed-cycle, vortex-stabilized, nuclear light bulb engine concept shown in Fig. 1.

The engine employs seven separate unit cavities. In each cavity, energy is transferred to seeded hydrogen propellant by thermal radiation from gaseous nuclear fuel suspended in a neon vortex. The vortex and propellant regions are separated by an internally cooled transparent wall. Neon is injected to drive the vortex, passes axially toward the end walls, and is removed through a port at the center of one or both end walls. The resulting fluid dynamic configuration is referred to as a "radial-inflow" vortex. The neon discharging from the cavity, along with any entrained fuel and fission products, is cooled by mixing with low-temperature neon, thus causing condensation of the nuclear fuel into liquid form. The liquid fuel is centrifugally separated from the neon and pumped back into the vortex region. The neon is further cooled and pumped back to drive the vortex. Further details of the design of the nuclear light bulb engine are presented in Ref. 1.

The analytical studies of the present investigation are divided into three categories: (1) criticality calculations, (2) nuclear kinetics studies, and (3) neutron and gamma ray heating calculations.

Criticality Calculations

Initial criticality calculations for the nuclear light bulb engine were reported in Ref. 2. One of the conclusions was that critical mass could be reduced substantially by a reduction in the amount of neutron-absorbing materials in the end walls and nozzle regions. Redesign of the nozzles and end walls was undertaken in the present study to eliminate wherever possible these neutron-absorbing structural materials. The primary objectives of the present investigation were (1) to evaluate the effects on U-233 critical mass of possible variations in engine design such as variations in the total mass and distribution of moderator materials, variations in the exhaust nozzle throat area, and variations in the amounts of neutron poisons in the propellant and moderator regions, (2) to evaluate factors affecting the dynamics of a nuclear light bulb engine such as prompt neutron lifetime, variations in nominal operating temperature and pressure, variations in fuel region radius, and fluctuations in fuel and propellant seed injection rates, and (3) to compare critical mass requirements using U-233 to the critical masses required for U-235 and Pu-239 in a reference nuclear light bulb engine.

Nuclear Kinetics Studies

In a nuclear light bulb engine, nuclear fuel is injected continuously into the active core volume. Experimental results from constant-temperature gas vortex tests indicate that the average residence time of nuclear fuel in a full-scale engine would probably be on the order of 20 sec. If this is the case, then delayed neutron precursors which emit delayed neutrons at time periods greater than 20 sec after the fission event would, on the average, contribute no neutrons to the active volume of the reactor core. This situation is quite similar to that for circulating fuel reactors; the important difference is that compressible gases are employed in the nuclear light bulb engine, whereas in circulating fuel reactors the fuel solution is an incompressible liquid. Thus, in the nuclear light bulb engine it is possible to have fluctuations in total fuel loading which result from fluid dynamic fluctuations in the heavy-gas residence time. Both the fraction of delayed neutrons which are lost from the active core and the total mass of nuclear fuel within the active core may vary with time. These are primary considerations in the overall control of the engine.

The primary objectives of the nuclear kinetics studies were (1) to formulate the neutron kinetics equations for a nuclear light bulb engine with variable loss rates of nuclear fuel and delayed neutron precursors, (2) to obtain solutions to these equations to determine responses to step, ramp, and oscillatory variations of both reactivity and fuel loss rate, and (3) to relate these responses to known properties affecting the dynamics of a nuclear light bulb engine such as the reactivity variations associated with changes in pressure, temperature, fuel region radius, nuclear fuel loading, and propellant seeding concentrations.

Neutron and Gamma Ray Heating Calculations

The ratio of beryllium oxide to graphite moderator weight chosen for criticality calculations was based on simplified one-dimensional heat balance calculations. It was assumed that neutron and gamma energy deposition was constant in the inner BeO regions and dropped off exponentially in the external BeO and graphite regions. Coolant circuit pressure drops, temperatures, and flow rates reported in Ref. 1 were also based on these assumptions for neutron and gamma energy deposition. In addition, studies of fiber-wound pressure vessels reported in Ref. 1 indicated that the nuclear radiation levels in the pressure vessel of a nuclear light bulb engine could potentially degrade the strength of a fiberglas laminate. Finally, since experimental measurements of the effects of radiation damage on the transmissivity of transparent wall materials have been performed and are being continued, it is desirable to make comparisons of the radiation environments of the full-scale nuclear light bulb engine and the various experimental radiation sources. Thus, it is necessary to perform detailed calculations of the neutron and gamma ray heating in all regions of a reference nuclear light bulb engine.

Neutron and gamma ray heating calculations were undertaken for a reference nuclear light bulb configuration with the objectives (1) to provide neutron and gamma ray heating estimates so that coolant circuit pressure, temperature, and flow conditions can be checked and adjusted where necessary, (2) to provide estimates of neutron and gamma ray dose rates and dosages in the transparent walls and to compare these with the radiation environments employed for past and present experimental measurements of the effects of radiation on transparent materials, and (3) to provide an estimate of the radiation dosages deposited in the fiber-wound pressure vessel of a full-scale engine and to evaluate the potential for degradation of pressure vessel strength due to radiation damage.

CRITICALITY CALCULATIONS

Review of Previous Studies

Initial criticality calculations were reported in Ref. 2 for the nuclear light bulb engine. A U-233 critical mass of 43.5 lb was determined for a reference engine on the basis of two-dimensional neutron transport theory. It was concluded that this critical mass could be reduced substantially be reduction of the amount of neutron absorbing materials in the end walls and by optimization of the amount of moderator material located in the end walls and between the seven unit cavities. These factors provided the motivation for studies of the effects of possible variations in engine design on U-233 critical mass.

Description of Reference Engine Configuration

A side-view sketch of the reference nuclear light bulb engine is shown in Fig. 1, and a cross-sectional view showing details of the unit cells is given in Fig. 2. The general characteristics of the reference engine are as follows:

1. There are seven separate unit cavities or cells with moderator material located between the cavities and surrounding the assembly of cavities.

2. The length of each cavity is 6 ft and the average diameter is about 2.3 ft; hence, the volume of all seven cavities is 169.8 ft^3 (equal to the volume of a single cavity having a diameter of 6 ft and a length of 6 ft).

3. The vortex volume (the volume within the transparent walls) for the seven cavities is equal to half of the total cavity volume, or 84.9 ft^3.

4. The cavity operating pressure is 500 atm.

5. The radius of the fuel-containment region is assumed to be 85% of the radius of the transparent wall.

6. The fuel radiating temperature is assumed to be 15,000 R.

7. The propellant exit temperature is assumed to be 80% of the fuel radiating temperature, or 12,000 R.

A fuel radiating temperature of 15,000 R produces a black body heat flux at the outside edge of the fuel-containment region of 24,300 Btu/sec-ft^2 which, for the total surface area of the seven fuel-containment regions (179.8 ft^2), produces a

total power of 4.37×10^6 Btu/sec or 4600 megw. The engine size and radiating temperature chosen provide an engine power approximately equal to that considered for advanced solid-core nuclear rockets.

Approximately 15% of the total fission energy created is dissipated by (1) energy deposition by neutrons and gamma rays in the moderator materials, (2) entrainment in fuel and neon separation and recirculation system, (3) convective heat transfer to the cavity walls by the hot hydrogen propellant, and (4) leakage of a small amount of energy from the engine boundaries. The hydrogen propellant must remove the heat from the moderator and recirculation system before injection into the cavity. Therefore, it is assumed that the hydrogen inlet enthalpy must be about 15% of the hydrogen exit enthalpy, or 15,500 Btu/lb, corresponding to a hydrogen inlet temperature of 4050 R. Tungsten particles are used (about 4% by weight) to seed the hydrogen propellant to make it sufficiently opaque to allow only 2% of the radiated energy to reach the cavity walls.

The basic cylindrical geometry used for nuclear calculations is shown in Fig. 3. The compositions of the various regions and total weights of materials employed in the reference engine are given in Tables I and II. The total weight of the engine in Table II, 72,407 lb is 6.5 percent less than the weight of the engine when the mid-section is tapered and end walls are rounded as in Fig. 1. By comparison, the reference engine described in Ref. 1 weighed 70,000 lb. The regions denoted as hot gases include hydrogen propellant, hydrogen and neon at lower temperatures to simulate relatively cool boundary layers adjacent to the transparent walls, the transparent walls (SiO_2) at 2000 R, and the cavity liner tubes at 1360 R. The cavity linear is made of internally cooled beryllium tubes coated with aluminum to provide high reflectivity for the incident thermal radiation. All of these materials, including the cavity liner, are homogenized into a single hot gas region for the nuclear calculations in order to conserve mesh points and computation time.

Additional regions which were homogenized to reduce computation time in two-dimensional calculations include the pump, heat exchanger, and plumbing region above the upper end walls; the upper and lower end walls; and the fiber-wound pressure vessel. Region 2 in Fig. 3 also contains steel structure to help carry gravitational loads on the reactor core. Unoccupied portions of region 2 are pressurized with hydrogen at 500 atm. The graphite and BeO upper end walls (regions 3 and 4 in Fig. 3, respectively) contain manifolds for coolant and propellant plus hafnium-shielded fuel injection and recirculation system ducts. Hafnium is employed to shield the fuel in the ducts from the high thermal neutron fluxes in these regions, thereby preventing excessive localized heating. The hafnium wall thicknesses for the ducts were chosen on the basis of previously reported calculations (Ref. 3). The BeO and graphite lower end walls (regions 14 and 15 in Fig. 3) contain the same materials as the radial outer BeO and outer graphite (regions 11 and 12) with a 10% reduction in volume fraction of solid material to allow for manifolds for collecting and turning moderator coolant flow.

It should be noted that the sectional view in Fig. 1 shows six nozzles. This results from a design which employs four nozzles per unit cavity so that no structural grid is required to support the bases of the transparent walls. Instead, loading support is supplied by the pressure vessel. The configuration shown in Fig. 3 employs only one central and one annular nozzle to reduce the geometric complexity of the end walls and thereby reduce the number of mesh points required to describe the radial geometry.

Approximately 5% of all moderator volume is devoted to small-diameter passages containing hydrogen coolant at 500 atm. Hydrogen is also present at a pressure of 250 atm and at a volume fraction of 0.20 between two layers of the fiber-wound pressure vessel to provide internal cooling. The BeO associated with each unit cavity contains, in addition to hydrogen coolant passages, SiO_2 ducting for distribution and circulation of the cavity liner and transparent-wall coolant, and internally cooled graphite-insulated beryllium tie rods. A flow divider and pyrolytic graphite insulating layer separates the outer hot graphite from the BeO associated with the unit cavities. These features are shown in Fig. 2.

Nuclear Analysis and Cross-Sections

The configuration shown in Fig. 3 contains adjacent zones with widely differing neutron scattering and absorption properties. Hence, a large number of mesh points are required for either neutron transport or diffusion theory calculations. To remain within the limits of reasonable computation time, the following steps were followed in the nuclear analysis.

All one-dimensional calculations were performed using the ANISN neutron transport theory code (Ref. 4). The geometry employed for one-dimensional calculations was that of a radial cross-section through the mid-plane of Fig. 3. First, the minimum order of angular quadrature was chosen to be S4 on the basis of previously calculated results (Ref. 2). This minimum order of quadrature was established by performing a series of one-dimensional, infinite-cylinder calculations for a unit cavity with the result that fluxes and eigenvalues remained essentially the same for S4, S6, and S8 angular quadratures.

It was necessary to employ several thermal neutron energy groups in the range from 0 to 1.125 ev to calculate the neutron absorptions and spectra accurately for adjacent regions in the moderator at quite different temperatures. In addition, to calculate the effects of neutron upscattering by the presence of hydrogen and hot neon at temperatures from 2000 to 12,000 R in the hot gas regions, it was necessary to add several thermal neutron groups in the range between 1 and 29 ev. The basic set of 24 neutron energy groups was chosen with 14 of the groups covering the range from 0 to 29 ev and the remaining groups covering the range from 29 to 10^7 ev. Table III contains the energy boundaries of the 24-group structure.

To calculate two-dimensional configurations economically, the 24-group cross-sections used in one-dimensional finite-cylinder calculations were used to generate volume- and flux-weighted 4-group cross-sections. The neutron energy boundaries of the 4-group set are also shown in Table III. The boundary between groups 3 and 4 in the 4-group set is at 8.32 ev, and some up-scattering of neutrons from group 4 to group 3 did occur. In order to eliminate up-scattering probabilities from the two-dimensional problems, the option in the ANISN code which subtracts the up-scattering from the down-scattering and thereby maintains the balance of transfer of neutrons between adjacent groups was used (Ref. 4). This created a 4-group cross-section set which had only down-scattering.

To ensure the accuracy of the 4-group cross-sections, they were reused in calculations for the same one-dimensional configuration from which they were generated, and comparisons of eigenvalues, fluxes, leakages, and absorptions by region were made with the original 24-group results. The values of the k_{eff} for the 4-group and 24-group calculations agreed to within 0.02 percent. Absorptions, leakages, and fluxes by group and region agreed to within at most 2.0% (Ref. 2). This close agreement verified that the 4-group cross-sections could be used for two-dimensional calculations.

Two-dimensional calculations were made using the 4-group cross-sections in the EXTERMINATOR-II neutron diffusion theory code (Ref. 5). One two-dimensional transport theory calculation was made for the reference nuclear light bulb engine of Fig. 3 using S4 angular quadrature in the DOT code (Ref. 6). Mesh spacings and 4-group cross-sections used for the two-dimensional neutron transport theory calculation were identical to those employed for the diffusion theory calculations so that an accurate comparison of results could be made.

To perform additional exploratory calculations economically, such as computation of the variation of critical mass with moderator temperature, it was necessary to establish a buckling correction for the one-dimensional cylindrical configuration. This correction was in the form of an effective cylinder height for the one-dimensional geometry consisting of the radial cross-section at the axial mid-plane of the configuration in Fig. 3. Once the effective cylinder height was established such that critical fuel loadings duplicated accurately those from the corresponding two-dimensional results, the above mentioned exploratory calculations were carried out using the one-dimensional ANISN code with 24 neutron energy groups.

The eigenvalue convergence criterion was $\leqq 0.0001$ for all one-dimensional calculations and $\leqq 0.0005$ for all two-dimensional calculations.

Fast neutron cross-sections were calculated using the GAM-I code with slowing-down spectra calculated for the various local moderator materials (Ref. 7). The slowing-down spectrum in the cavity regions was assumed to be that of the beryllium

oxide moderator, the material in largest quantity adjacent to the cavities. Thermal neutron absorption cross-sections were calculated using the TEMPEST code with spectra again chosen for the temperature and materials of the local moderator regions (Ref. 8). Up- and down-scattering probabilities within the thermal neutron energy groups were calculated using the SOPHIST-I code (Ref. 9). This code includes the enhancement of reaction rates due to relative velocity between neutron and scatterer; this effect was included in the calculation of the transport cross-section for the various materials.

Treatment of the transport cross-section in the special cases of atomic and molecular hydrogen and hot neon follows that reported in earlier calculations with the addition of dependence of the scattering cross-section of molecular hydrogen on the energy of interaction, a function of relative velocity (Refs. 2 and 10). The equation for the transport corss-section is

$$\sigma_{tr}^{i} = \sigma_{a}^{i} + \left(\sum_{j=1}^{13} \mu_{ij}\right) \sigma_{s}^{i} \left(1 - \overline{\cos\theta}\right)^{i} \qquad (1)$$

The sum of μ_{ij} is the sum of the up- and down-scattering probabilities from energy group i to all energy group j; $\overline{\cos\theta}$ is the mean value of the cosine of the scattering angle (which includes consideration of the motion of the scatter as well as the incident neutron); and σ_{s}^{i} allows for the relative velocity dependence necessary to correct for the effects of molecular binding on the scattering cross-section at low interaction energies (Ref. 10).

Results of Criticality Calculations

Effects of Variations in Engine Design

The nuclear, fluid dynamic, heat transfer, and performance characteristics of the engine interact so as to provide a wide range of design possibilities. One of the objectives of this study was to evaluate the effects of possible variations in reference engine design on the U-233 critical mass. The effects considered include variation in the total mass and distribution of moderator material, variations in the exhaust nozzle throat area, variations in the amount of tungsten seed material in the hydrogen propellant, and variations in the total mass of hafnium employed to shield fuel injection and recirculation system ducts.

Two-dimensional neutron diffusion theory calculations were performed in which the size and compositions of the gaseous regions remained the same but in which the total mass of moderator material was reduced. The ratio of BeO to graphite moderator weight was chosen for each of these configurations on the basis of simplified one-dimensional heat balance calculations in which it was assumed that neutron and gamma

energy deposition was constant in the inner BeO regions and dropped off exponentially in the external BeO and graphite regions. The ratio of radial moderator mass to total moderator mass was assumed to be 0.5. The term radial moderator mass refers to all moderator mass between the upper and lower end walls in Fig. 3 (i.e., regions 7, 11, and 12). The remaining moderator material beyond the ends of the unit cavities is referred to as end-wall moderator mass (i.e., regions 3, 4, 14, and 15). The internal moderation factor, f_{IM}, was 0.143. The internal moderation factor is the ratio of inner BeO mass (region 7 in Fig. 3) to the total BeO mass in the entire engine (regions 4, 7, 11, and 14). Normally, the inner BeO would contain all the BeO associated with the inner unit cavity and half of the BeO associated with the six outer cavities, in which case the internal moderation faction would be 0.286. An internal moderation factor of 0.143 means that half of the BeO which would normally be located in the inner BeO region has been shifted outward to the outer BeO region. It is shown later that changes in the BeO distribution can be made to minimize critical mass and, more importantly, to balance the rate of power output per unit cavity between the inner and outer cavities.

The results of the calculations to investigate the effects of total moderator mass on critical mass are shown in Fig. 4. A decrease in total moderator mass from 39,000 to 24,600 lb results in an increase in U-233 critical mass from 34.7 to 43.8 lb. In comparison, the total moderator mass in the configuration employed in Ref. 2 was 33,100 lb and U-233 critical mass was 43.5 lb.

One-dimensional, 4-group transport theory calculations were performed to investigate the effect of varying the amount of internal moderation. An effective cylinder height was chosen such that the critical fuel loading matched that from the earlier two-dimensional result, and the internal moderation factor, f_{IM}, was varied between 0 and 0.286. The results of these calculations are shown in Fig. 5. Critical mass is minimum at $f_{IM} = 0.190$. The reference engine was chosen to have a value of f_{IM} of 0.143 because the ratio of power per unit cavity between the inner and outer cavities would be closer to unity with relatively little increase in critical mass. This ratio, P_I/P_O, is also shown in Fig. 5 with one point of comparison for the reference engine from the two-dimensional diffusion theory results. Further reduction in P_I/P_O from 1.14 to 1.0 would have to be achieved by different fuel loadings in the inner and outer cavities. The reduction in critical mass from $f_{IM} = 0$ to the minimum point at $f_{IM} = 0.190$ was about 5%.

Another factor affecting critical mass is the distribution of moderator mass between radial and axial directions. The results of two-dimensional diffusion theory calculations performed to evaluate the effect of varying the fraction of total moderator mass used in the radial direction, f_{RM}, are shown in Fig. 6. Critical mass is a minimum at $f_{RM} = 0.5$.

A final series of two-dimensional diffusion theory calculations was performed to evaluate the effect on critical mass of varying the effective nozzle throat area, A_T, in the reference engine. The results of these calculations are shown in Fig. 7, in which it is noted that the ratio of the fractional change in critical mass to the fractional change in effective area of nozzle throat is $(\Delta M/M_C)/(\Delta A_T/A_{T_O}) = +0.156$ at the reference engine design point. At the point where $A_T = 0$, only the nozzle throat was closed off with the nozzle approach still in the BeO portion of the lower end wall (region 14 in Fig. 3). The nozzle approach and throat areas of the reference engine were calculated on the basis of splitting the nozzle volume between the lower BeO, the lower graphite, and the pressure vessel regions with the assumption that the nozzle radius varied linearly with distance from the base of the unit cell to the outside edge of the pressure vessel. The actual nozzle throat area per unit cell was 0.006 ft^2, as reported in Ref. 1. The relatively large effective nozzle throat area of 2.1 ft^2 employed in the reference engine calculations was chosen to allow for the effects of structure and coolant manifolds around the nozzle throats.

The reference engine selected has a U-233 critical mass of 34.7 lb. This mass corresponds to an average fuel partial pressure in the fuel-containment region of 200 atm on the basis of the studies of Ref. 11.

Material worths were calculated using the EXTERMINATOR-II adjoint and perturbation calculation options. Table IV contains the results of these calculations in the form of reactivity coefficients. These coefficients were used to estimate the effects on critical mass to be expected (1) from tungsten seed in the hydrogen propellant (4% by weight), and (2) from reduction in the size of the hafnium-shielded fuel injection and recirculation system ducts in the upper end walls. Tungsten seed was included in the two-dimensional diffusion theory calculations in only trace amounts in the nozzle regions and in the hydrogen propellant. Applying the reactivity coefficients of Table IV to the inclusion of tungsten in the amount of 4% by weight of the hydrogen propellant would decrease k_{eff} by 0.001, which would result in an increase in critical mass of 0.09 lb.

The major portion of the hafnium in the upper end walls is due to fuel recirculation system ducts which were assumed to require twelve times the flow area of the fuel injection ducts to accommodate the neon bypass flow required to cool the recirculating fuel. If this flow area were halved, the required hafnium mass in the end wall would be reduced by about 30%, k_{eff} would increase by 0.004, and critical mass would decrease by 0.36 lb. The hafnium duct walls in the upper end wall were assumed to be 0.2 in. thick, and the hafnium cross-sections employed in all calculations had self-shielding factors applied to them (Ref. 12).

Factors Affecting Dynamics of a Nuclear Light Bulb Engine

There are several factors such as temperature and pressure variations, fuel radius changes, and fluctuations in fuel and tungsten seed injection which can affect the reactivity of any type of gaseous nuclear rocket engine. Some of these factors have been investigated using the EXTERMINATOR-II adjoint-perturbation calculations and one-dimensional 24-group transport theory calculations for the reference nuclear light bulb engine.

The reference engine has different nominal operating temperatures, T_o, in different regions as shown in Tables I and II. Variations in operating temperature were simulated by varying the nominal operating temperature of each region simultaneously between 0.8 T_o and 1.2 T_o. In gaseous regions, pressure was assumed to be constant at 500 atm during the variation in operating temperature. Calculations of the effects of these temperature variations were performed using one-dimensional, 24-group transport theory with an effective cylinder height of 620 cm. The results of the calculations are shown in Fig. 8. There is a positive temperature coefficient of reactivity at T_o, with the slope falling off at 1.2 T_o. Table IV contains the linearized value of the temperature reactivity coefficient near T_o. The reason for the positive temperature reactivity coefficient can be seen by comparing the curve of average fission cross-section for group 4 with the curve showing a 1/v variation. It should be emphasized that changes in density which occur as a result of a variation of temperature of the hot gases at constant pressure cause axial leakage variations which cannot be accurately accounted for in a one-dimensional calculation. Eventually, the effects of increased axial leakage must overcome the positive reactivity contribution due to the non-1/v nature of the U-233 fission cross-section. Evaluation of the temperature at which the slope of the temperature coefficient of reactivity changes sign should be the subject of further two-dimensional calculations.

The hydrogen propellant regions of the reference engine contain relatively cool boundary layers near the cavity walls and transparent walls. The thicknesses of these layers affect the mixed mean temperature, T_{MM}, of the propellant. Calculations using the one-dimensional transport theory model described above were performed to evaluate the effect on reactivity due to variations in T_{MM} resulting from variations in the thicknesses of the relatively cool boundary layers. A positive reactivity coefficient shown in Table IV of $(\Delta k/k)/(\Delta T_{MM}/T_{MM_o}) = +0.0544$ resulted for variation of T_{MM} about a basic value of $T_{MM_o} = 5100$ R. This positive reactivity coefficient is explained by the non-1/v behavior of the group 4 fission cross-section as discussed above.

A final set of one-dimensional neutron transport theory calculations was carried out to determine the effect of fuel region radius variation for the reference engine configuration using an infinite cylinder height. Infinite cylinder height was used to eliminate possible variations in simulated axial leakages with the changes in

fuel density resulting from changes in fuel volume. Total and local pressure in the chamber and nuclear fuel mass were held constant as fuel region radius was changed. The results of these calculations yielded increases in reactivity with decreases in fuel radius over the range of fuel-to-cavity radius ratio of 0.5 to 0.61. The coefficient of reactivity, $(\Delta k/k)(\Delta R_F/R_F) = -0.0413$, is shown in Table IV. This result is contrary to what should be expected on the basis of self-shielding arguments. However, the self-shielding is so slight that it is over-ridden by the change in the non-1/v U-233 average fission cross section caused when thermal neutrons traverse the layer of neon at 15,000 R which increases in thickness as the fuel cloud is reduced in size.

The reactivity coefficients resulting from changes in the amount of tungsten seed in the hydrogen propellant and changes in the amount of hafnium in the upper end walls have been discussed previously and are also shown in Table IV. The reactivity coefficient associated with all gases in all regions, obtained from the results of the two-dimensional adjoint-perturbation calculations, is also shown in Table IV. This reactivity coefficient can be interpreted as the pressure coefficient of reactivity and has a positive value of $(\Delta k/k)/(\Delta P_c/P_{c_o}) = +0.0859$.

Prompt neutron lifetime was calculated for U-233 in the reference engine using the EXTERMINATOR-II adjoint-perturbation calculation. The result gave a prompt neutron lifetime of 0.516 msec.

Comparisons of Nuclear Fuels and Analytical Techniques

Two special one-dimensional, 24-group, neutron transport theory calculations were performed using the effective cylinder height of 620 cm to determine the required critical masses of Pu-239 and U-235 in the reference engine configuration. The results gave critical masses of 46.0 lb for Pu-239 and 50.4 lb for U-235. The corresponding critical mass for U-233 was 34.7 lb. The higher critical mass for U-235 compared with U-233 is due to both a lower average thermal fission cross-section and a lower yield of neutrons per fission. In the case of Pu-239, the fission/absorption resonance at 0.3 ev gives rise to a substantially higher thermal neutron fission cross-section but also a larger capture of fission ratio. Most important, the resonance cross-sections become self-shielded, causing the critical mass to be substantially higher than that required for U-233.

For purposes of comparison, one two-dimensional neutron transport theory calculation using the DOT code was performed using 4-group cross-sections and mesh spacings identical to those used in the two-dimensional diffusion theory calculations for the reference engine. The results from transport theory yielded a critical mass of U-233 of 30.90 lb, which is 11% lower than that from diffusion

theory. This critical mass corresponds to an average fuel partial pressure of 175 atm in the fuel-containment region on the basis of the studies of Ref. 11. The transport theory result had about half as much total neutron leakage from the system as was calculated by diffusion theory, and the radial neutron flux plots differed somewhat in the outer BeO and graphite regions. This can be seen in Fig. 9 where comparisons of the normalized radial neutron fluxes from one- and two-dimensional transport theory and two-dimensional diffusion theory are presented.

Neutron spectra are shown in Fig. 10 for the various regions of the reference engine. These spectra were plotted from the 24-group, one-dimensional transport theory results and were used primarily as a check for the thermal neutron scattering matrices. The effects of up-scattering by the hot gases can be seen in the relatively higher flux levels above 0.5 ev in the outer fuel region spectrum.

Recommendations for Future Research

Further analysis should be performed in three areas covered by the criticality calculations of this study: (1) a more detailed geometric model of the thrust nozzle end wall should be employed for two-dimensional analysis of the reference configuration, (2) two-dimensional calculations of the reactivity variations associated with changes in nominal operating temperature should be made, and (3) two-dimensional calculations of the reactive variations associated with changes in fuel region radius should be made.

U-233 critical mass requirements were shown to be quite sensitive to the choice of effective nozzle throat area. A series of two-dimensional calculations should be performed, using diffusion theory primarily, in which the lower end wall is divided into progressively greater numbers of axial zones until the nuclear model describes the effect of thrust nozzles on critical mass to the desired accuracy.

As described previously, gas density changes occur when changes in nominal operating temperature are applied under constant pressure conditions. This gives rise to variations in axial leakage which can be evaluated only by two-dimensional calculations. In addition, the present study analyzed reactivity variations resulting from fractional changes in material temperatures occurring simultaneously throughout the system. Since there are substantial differences in total masses and specific heats of the materials employed in the engine, a more realistic approach would allow different time histories in the temperature response to a sustained step change in power level. It is recommended therefore, that further analyses of the temperature coefficient of reactivity be conducted using two-dimensional diffusion theory to allow for axial leakage effects. These calculations should be done for several points in time following a sustained step change in power level in which material temperatures in the various regions are based on realistic temperature response time histories.

The calculations of variations in reactivity due to changes in fuel region radius should be expanded to include two-dimensional R-θ calculations to determine whether a more accurate geometric description of the reference engine geometry in the cross-sectional plane has a significant effect on the results. In addition, evaluation of the reactivity coefficient associated with changes in fuel region radius should be performed for cases in which compression and expansion of the fuel cloud occur so rapidly that local pressures do not remain constant, but vary in proportion to local fuel density.

NUCLEAR KINETICS STUDIES

Nuclear Kinetic Equations with Variable Fuel Residence Time

The principal unusual factor in the kinetic behavior of a nuclear light bulb engine is that the nuclear fuel is injected continuously into the active core volume. Experimental results for constant-temperature gas vortex tests indicate that the average residence time of nuclear fuel in a full-scale nuclear light bulb engine would probably be on the order of 20 sec. If this is the case, then delayed neutron precursors which emit delayed neutrons at time periods greater than 20 sec after the fission event would contribute essentially no neutrons to the active volume of the reactor core. This problem is quite similar to that for circulating fuel reactors; the important difference is that compressible gases are employed in a nuclear light bulb engine, whereas in the circulating fuel reactors the fuel solution is an incompressible liquid. Due to compressibility, it is possible to have fluctuations in total fuel loadings which result from fluid dynamic fluctuations in the heavy-gas residence time. Thus, both the fraction of delayed neutrons which are lost from the active core and the total mass of nuclear fuel within the active core will vary with time. These are primary considerations in the overall control of the engine.

The equations describing the space-independent kinetics of a nuclear light bulb engine are shown in Fig. 11. Equation (a) determines the neutron level; it includes a time-varying reactivity coefficient which is affected by the rate of change of nuclear fuel mass described in Eq. (c) of Fig. 11. Equation (d) gives the reactivity feedback which results from time variations in nuclear fuel loading. The rate of change of reactivity with fractional change in critical mass is taken from Table IV. It can be seen in Eq. (d) that a δk_o term is present. This term is the steady-state reactivity required to overcome the loss of delayed neutrons due to a finite residence time of delayed neutron precursors in the reactor core. Equation (e) is the equation for δk_o, the necessary steady-state reactivity for a given fuel and delayed neutron precursor loss rate. Equation (e) was derived in accordance with Ref. 13. Equation (b) (six different equations) describes the time behavior of the six groups of delayed neutron precursors. In these equations it is assumed that the delayed neutron precursors have the same residence time as the nuclear fuel. Thus, the feedback due to variations in the nuclear fuel residence time include variations in the delayed neutron fractions which are emitted in the reactor core as well as a direct reactivity feedback due to variations in nuclear fuel mass with variations in the fuel residence time.

The equations shown in Fig. 11 were programmed for the UNIVAC 1108 computer for the reference nuclear light bulb engine. In the reference engine the fuel decay constant is assumed to be 0.05 sec^{-1}; (fuel decay constant, λ_{F_o}, is the inverse of average fuel residence time) the critical fuel loading, 34.7 of U-233; and the rate of change of reactivity with fractional change in mass, 0.384. Table V contains the delayed neutron yields for U-233 which were employed in these calculations. These delayed neutron yields are from Ref. 14.

Results of Nuclear Kinetics Studies

Responses to Step and Ramp Changes in Reactivity and Fuel Residence Time

The power level of the nuclear light bulb is directly proportional to the neutron level. Power level responses to step and ramp changes in reactivity for a fixed nuclear fuel decay constant ($\lambda_{F_o} = 0.05\ sec^{-1}$) are shown in Fig. 12. The prompt neutron lifetime was 5×10^{-4} sec and the steady-state reactivity required to compensate for the loss of the delayed neutrons was $\delta k_o = 0.030\beta$, where β is the total delayed neutron fraction for U-233. It can be seen from Fig. 12a that the power level doubling time for sustained step insertion of reactivity of $+0.20\ \beta$ was about 4 sec. For sustained ramp insertion of reactivity of $0.20\beta\ (t-t_o)$, Fig. 12b, the power level doubling time was about 2 sec. These two results will be used in the following discussion as a basis for comparisons when initial fuel decay constant and prompt neutron lifetime are varied.

Power level responses to positive step and ramp changes in reactivity for different values of fuel decay constant are shown in Fig. 13a and 13b, respectively. Prompt neutron lifetime was held constant at 5×10^{-4} sec for these cases. Power level doubling times for sustained step insertions of reactivity of 0.20β were 0.85, 3.9, and 14.4 sec for fuel decay constants of 1.0, 0.05, and 0.0 sec^{-1} (corresponding to average fuel residence times of 1.0, 2.0, and ∞ sec), respectively. For sustained ramp insertions of reactivity of $0.20\beta\ (t-t_o)$, power level doubling times were 1.5, 2.0, and 2.5 sec for fuel decay constants of 1.0, 0.05, and 0.0 sec^{-1}, respectively.

Figure 14 shows power level responses to step and ramp changes in reactivity for different values of prompt neutron lifetime while fuel decay constant was held constant at 0.05 sec^{-1}. Power level doubling times for sustained step insertions of reactivity of 0.20β were 9.4, 3.9, and 3.0 sec for prompt neutron lifetimes of 3×10^{-3}, 5×10^{-4}, and 10^{-4} sec, respectively. For sustained ramp insertions of reactivity of $0.20\beta\ (t-t_o)$, power level doubling times were 3.5, 2.0, and 1.0 for prompt neutron lifetimes of 3×10^{-3}, 5×10^{-4}, and 10^{-4}, respectively.

It is interesting to examine the variations in fuel loading and power level with variations in fuel decay constant. Figure 15 presents the fractional variations in fuel loading which occur following step changes in fuel decay constant for the reference engine; Fig. 16 presents the same information for ramp changes. In both cases the prompt neutron lifetime was 5×10^{-4} sec and the initial fuel decay constant was 0.05 sec^{-1}. The fractional mass variations terminated abruptly in these figures because the coupled neutron level response had reached some limiting value specified in the input of the digital computer program.

Figure 17 shows the corresponding variations of power level. The power level doubling times for sustained step changes of fuel decay constant of $-1.0\,\lambda_{F_o}$, $-0.10\,\lambda_{F_o}$, and $-0.01\,\lambda_{F_o}$ sec^{-1} were 0.15, 0.65, and 3.30 sec, respectively (Fig. 17a). For sustained ramp changes of fuel decay constant of $-1.0\,\lambda_{F_o}(t-t_o)$, $-0.10\,\lambda_{F_o}(t-t_o)$, and $-0.01\,\lambda_{F_o}(t-t_o)$ sec^{-1}, the power level doubling times were 0.50, 1.15, and 2.90 sec, respectively (Fig. 17b). The power level response to sustained ramp changes of $-0.01\,\lambda_{F_o}(t-t_o)$ sec^{-1} will be used below as a basis for comparison with power level responses when the initial value of fuel decay constant and the prompt neutron lifetime are varied.

Figure 18 presents the variation of fuel loading with negative ramp changes in fuel decay constant for different initial values of fuel decay constant ranging from 1.0 to 0.01 sec^{-1}. The effects of these variations on power level are shown in Fig. 19a. Power level doubling times for sustained ramp changes of fuel decay constant of $-0.01\,\lambda_{F_o}(t-t_o)$ sec^{-1} were 4.75, 2.90, and 0.85 sec for initial values of fuel decay constant, λ_{F_o}, of 0.02, 0.05, and 1.0 sec^{-1}, respectively. Prompt neutron lifetime was 5×10^{-4} sec for these cases. Figure 19b shows power level response to sustained ramp changes in fuel decay constant of $-0.01\,\lambda_{F_o}(t-t_o)$ sec^{-1} for different prompt neutron lifetimes with the initial value of λ_{F_o} held constant at 0.05 sec^{-1}. Power level doubling times were 2.55, 2.90, and 4.2 sec for prompt neutron lifetimes of 10^{-4}, 5×10^{-4}, and 3×10^{-3} sec, respectively.

Response to Oscillations in Reactivity and Fuel Residence Time

The solutions to the neutron kinetic equations discussed thus far are pertinent when considering gross changes in power level, neutron level excursions, and some aspects of reactor start-up. Responses to small perturbations in reactivity or fuel decay constant must also be evaluated. This can be accomplished by developing an analytical transfer function for the system of equations and solving for neutron level responses to reactivity or fuel decay constant perturbations of various forms. As an initial step in the development of such a system transfer function, the nuclear kinetics program included an option to introduce sinusoidal oscillations in either reactivity or fuel decay constant. Solutions to the neutron level equations provide data to determine the gain in neutron level oscillation amplitude

relative to the amplitude of the perturbing oscillation and the phase differences between the perturbing oscillations and the neutron level response. Gain in decibels in this study is defined as $20 \log_{10}\left[(\Delta n/n_o)/(\delta k/k)\right]$ or $20 \log_{10}\left[(\Delta n/n_o)/(\delta \lambda_F/\lambda_{F_o})\right]$.

Small perturbations in reactivity of $0.10\ \beta \sin \omega t$ and in fuel decay constant of $0.0\ \lambda_{F_o} \sin \omega t$ sec^{-1} were applied to the neutron kinetic equations over a frequency range from 10^{-1} to 1000 radians/sec for values of initial fuel decay constant of 0.05 sec^{-1} and 0.50 sec^{-1}. Prompt neutron lifetime was 5×10^{-4} sec for all cases.

Gain and phase responses to reactivity oscillations are shown in Fig. 20. For an initial value of fuel decay constant of 0.05 sec^{-1}, the gain in the amplitude of neutron level oscillations relative to the amplitude of oscillations in reactivity was about 83 db for frequencies below 3.0 rad/sec; it decreased at a rate of 20 db/decade for frequencies above 3.0 rad/sec. The phase difference reached a minimum of -30 deg at about 0.5 rad/sec and approached an asymptotic value of -90 deg above 50 rad/sec. The principal effect of changing the initial value of the fuel decay constant from 0.05 to 0.50 sec^{-1} was to increase the gain in neutron level response by about 20 db throughout the frequency range of interest.

Figure 21 presents the gain and phase response to oscillations in fuel decay constant. For an initial value of fuel decay constant of 0.05 sec^{-1}, the gain in the amplitude of neutron level oscillations relative to the amplitude of oscillations in fuel decay constant was about 32 db at 0.3 rad/sec; it decreased at a rate of 40 db/decade for frequencies above 3.0 rad/sec. The phase difference was about -110 deg at frequencies below 0.3 rad/sec and approached an asymptotic value of -180 deg above 50 rad/sec. The latter -180 deg phase difference is not expected to cause instabilities because gain is of the order of -40 db at 50 rad/sec. As was the case for response to reactivity oscillations, the principal effect of changing the initial value of fuel decay constant from 0.05 to 0.5 sec^{-1} was to increase the gain in neutron level response by about 20 db over all frequencies.

The reactivity coefficients in Table IV are related to perturbations in reactivity as follows: A ± 1% variation in operating pressure, P_c, mixed-mean gas temperature, T_{MM}, nominal operating temperature, T_o, or fuel region radius, R_F, would result in reactivity perturbations of $\pm 0.343\beta$, $\pm 0.218\beta$, $\pm 0.180\beta$, and $\pm 0.165\beta$, respectively. All of these are of amplitudes great enough to cause large responses in neutron level at low frequencies. However, a preliminary analysis indicates that the gas densities and chamber dimensions are such that resonant oscillations are not likely to be excited below several hundred rad/sec. Dynamic responses of engine parameters such as temperature, pressure, fuel cloud radius, fuel loss rate, and power level require further investigation, expecially in the frequency domains in which resonant response phenomena are possible.

Recommendations for Future Research

The nuclear kinetic behavior discussed in the preceding pages is only a small part of the entire nuclear light bulb engine kinetics. The principles of operation of the engine as conceived in the engine design studies of Ref. 1, have been described previously. The various coolant, propellant, and fuel separation and recirculation systems are coupled with the neutron equations through temperature and pressure response to neutron level changes, and they are coupled with one another through the heat exchangers and system pressure and temperature variations. The equations governing these relationships for small perturbations about a nominal steady-state power level should be derived and included with the nuclear equations to create a general engine simulation. To simplify such a simulation, transfer functions for the various subsystems should be developed. An analytical transfer function for the neutron kinetics equations has recently been derived and is being verified using the complete digital computer solutions for the nonlinear problem.

The engine kinetics simulation should be directed toward determining (1) stability of the engine at normal full-power operating conditions, (2) fuel control requirements and their relation to the average fuel residence time, (3) sensors and other controls that may be required to provide stability, (4) engine response to small changes in fuel flow rate, (5) temperature and pressure transients in the moderator, fuel region, propellant region, and transparent walls, and (6) transient loadings in the fuel and neon separation and recirculation system. Parameter variations should be made to determine the parameters to which the system is most sensitive.

NEUTRON AND GAMMA RAY HEATING CALCULATIONS

Engine Configuration and Analytical Technique

Neutron and gamma ray heating calculations were performed for the reference nuclear light bulb engine. The nuclear model for the calculation of neutron and gamma ray fluxes and energy deposition rates was the cylindrically symmetric configuration shown in Fig. 3 and described in Tables I and II (the same geometry that was used for criticality calculations). The calculations were carried out using the QADHD code described in Ref. 15. The program is written to calculate gamma and fast neutron radiation from a volume-distributed source having cylindrical symmetry in a complex source-shield geometry. Point kernel methods are employed, using attenuation coefficients and infinite-medium buildup factors for gamma ray penetration and neutron removal cross-sections for fast neutron penetration. Gamma ray source spectra are specified by input, and fast neutron spectra are those from neutron moments method calculations for point fission sources in infinite media of light water, beryllium, or graphite. Gamma ray attenuation coefficients, buildup factors, and neutron removal cross-sections for all elements are contained within the code.

It was necessary to make several choices of data to perform the calculations. These choices include (1) selection of gamma and neutron spectra in each environment, (2) an estimate of the total delayed gamma energy released by fission fragments during the approximate period in which they are within the active volume of the engine, (3) calculation of neutron elastic scattering cross-sections and average energy loss per collision, and (4) selection of gamma energy absorption coefficients.

Neutron and Gamma Ray Spectra and Cross-Sections

The fission fragment average residence time in the engine is estimated to be of the order of 20 sec. Therefore, it was assumed that the most appropriate gamma spectrum for dose calculations would be that for prompt gamma rays. However, as shown in Fig. 22, in the 20 sec after fission about 1.5 mev in gamma energy is released by fission fragments. The data in Fig. 22 for the delayed energy release by beta decay and gamma emission from fission fragments was taken from reports of experimental measurements in Refs. 16 and 17. It was assumed that the gamma rays emitted short times after fission would have a spectrum approximately the same as that for prompt gammas. The spectrum employed for gamma dose calculations was the spectrum for prompt gamma rays enhanced at each energy interval in direct proportion to the ratio of the integrated prompt plus delayed gamma energy released 20 sec after fission to the integrated prompt gamma energy release alone. The gamma energy group structure, the prompt gamma spectrum, and the normalized spectrum employed in the calculations are shown in Table VI. The prompt gamma spectrum was taken from Ref. 18.

It can be seen that beryllium oxide is the dominant moderator material in the core regions of the cylindrically symmetric configuration shown in Fig. 3. For this reason, the neutron spectrum for a point isotropic U-235 fission source in an infinite beryllium medium was chosen as the spectrum to be used for the neutron dose calculations. These spectra were obtained from the moments calculations of Ref. 19 and were internal to the QADHD code described in Ref. 15.

The neutron heating rates and dosages deposited in the materials are a result primarily of elastic scattering of fast neutrons. The elastic scattering cross-sections were calculated using the GAM-I fast neutron cross-section code described in Ref. 7. It was assumed that the average energy degradation per scattering event, $\overline{\Delta E}$, was given by

$$\overline{\Delta E} = E_i \left[2A/(1 + A)^2 \right] (1 - \overline{\cos\theta}) \qquad (2)$$

where E_i is the average neutron energy in group i, A is the atomic weight of the scattering element, and $\overline{\cos\theta}$ is the average cosine of the scattering angle in the center of mass coordinate system. Table VII contains the scattering cross-sections and average energy degradation per group used for the calculation of neutron heating and dosages.

The gamma energy absorption coefficients were obtained from Ref. 18. Values of these coefficients over the energy range from 0.5 to 10 mev are shown in Table VIII. The gamma fluxes calculated in the QADHD code were obtained with the use of the light water buildup factors.

Results of Neutron and Gamma Ray Heating Calculations

Neutron and Gamma Ray Heating in Different Regions

Results are presented in Table IX for three different average fuel residence times (1.0, 20.0, and 60.0 sec). For these average fuel residence times, the fission fragment and beta energy release rates in the fuel regions were 4036, 4131.6, and 4147.6 megw, respectively. The corresponding neutron and gamma ray energy release rates in the active core were estimated to be 296, 325, and 342 megw, respectively, and the corresponding rates of energy release from delayed beta particles and gamma rays in the fuel separation and recirculation system were estimated to be 268, 143.5, and 110.5 megw, respectively. It was assumed that all of the fission fragments were separated from the fuel in the fuel separation and recirculation system and that the delayed gamma ray energy was totally absorbed by the heavy metals in the turbine, pumps, heat exchangers, plumbing, and support structure in the upper end wall of

the pressure vessel. It was also assumed that the delayed beta decay energy was absorbed within the working fluid or inner piping surfaces of the fuel separation and recirculation system. Therefore, two heat exchanger region heating rates are shown in Table IX; one is for heating from neutron and gamma sources in the active core and one is for the heating due to delayed gamma rays and beta particles within the fuel separation and recirculation system. In all cases, total volumetric heating rates were normalized such that the neutron energy release rate was 117 megw, and the gamma ray energy release rate was 303 megw, for a total of 420 megw. Self-absorption of energy by the nuclear fuel was neglected.

The distribution of power deposited in various components for a total engine power of 4600 megw and an average fuel residence time of 20 sec was calculated to be as follows: fuel region, 4131.6 megw; moderator region, 210.6 megw; heat exhanger region, 144 megw; hot gas region between fuel and cavity walls, 74.9 megw (including 58.7 megw in the hydrogen propellant); pressure shell, 17.4 megw; and leakage out of reactor, 21.5 megw.

One of the principal results of the neutron and gamma ray heating calculations was the strong sensitivity to changes in average fuel residence time. As discussed above, it is assumed that the delayed energy release from fission is shared between the active core and the fuel separation and recirculation system such that the total delayed energy release is constant. The fuel recirculation system heat load due to both delayed gamma rays and beta particles varies from 268 to 110.5 megw as average fuel residence time varies from 1.0 to 60 sec. In comparison, the heat load in the moderator and structure, plus some leakage, varies only from 296 to 342 megw. Note that these energy release rates do not equal the 420 megw total quoted above because of the addition of delayed beta energy release to the recirculation system. The most desirable inlet condition to maintain as stable as possible is the transparent wall coolant injection temperature. The present coolant circuit design (see schematic diagram in Fig. 8 of Ref. 1) places a neon-hydrogen heat exchanger in a position to couple variations in fuel recirculation system heat loads directly to the transparent-wall coolant inlet conditions. Furthermore, heat loads in the fuel and neon separation and recirculation system are greater than assumed in Ref. 1 while heat loads to the bulk beryllium oxide and graphite moderator are smaller than assumed in Ref. 1. Further engine design work will be required to arrange the heat exchanger positions in the coolant circuit system and possibly alter the sequence of cooling various engine components in order to maintain coolant inlet and outlet temperatures at the desired levels throughout the system.

Two other results of interest were (1) the magnitudes of energy leakage from the system and (2) the amounts of direct heating, principally by neutrons of hydrogen propellant in the hot-gas regions. The rate of energy leakage from the entire system was calculated to be 6.2 megw for neutrons and 13.2, 15.3, and 16.6 megw for gamma rays for average fuel residence times of 1.0, 20, and 60 sec, respectively. Direct

heating of hydrogen propellant located between the fuel regions and cavity walls by neutron energy degradation was calculated to be 54.3 megw. This can be verified approximately by considering the cross-section for energy degradation for 2.0 mev neutrons from Table VII in which $\overline{\Delta E}\Sigma_S = 0.016$ mev/cm for hydrogen at 4000 R under 500 atm pressure. The mixed mean hydrogen temperature in the hot gases was calculated to be about 5100 R and the mean first-flight track length across the hot gas regions for neutrons emitted isotropically should be of the order of $\bar{l} = 45$ cm. Assuming 2.5 neutrons are emitted per fission, that the neutron energy released per fission is 4.9 mev, and that the total rate of neutron energy release is 117 megw, the energy deposited in hydrogen by first flight traversals of the hot gases should be given by $\bar{l}\Sigma_S\overline{\Delta E} = (4000/5100)(2.5)(117/4.9)(45)(0.016) = 34$ megw. The additional energy deposition results from additional traversals of the hot gas regions and from the proportionately larger energy degradation per collision for neutrons in the high-energy end of the neutron spectrum relative to lower-energy neutrons (see Table VII).

Transparent-Wall Dosages and Comparison with Reactor Tests

An experimental program has been under way for several years at UARL to determine the optical absorption properties of candidate materials for the nuclear light bulb transparent walls in a neutron and gamma ray radiation environment. Optical absorption measurements have been made for various samples after irradiation in the Union Carbide test reactor and during irradiation in a TRIGA test reactor (Refs. 20, 21, 22, and 23). The present calculations were performed to obtain a better estimate than previously available of the level of gamma and neutron dosages to which the transparent walls in a full-scale nuclear light bulb engine would be exposed, and to compare these with the dosages reported for the reactor irradiations.

The neutron heating and dose rates deposited in the nuclear light bulb transparent wall are shown in Table X. These results are for the midplane of the center cell of the seven unit cells (Fig. 3). The neutrons passing through the internal transparent wall of the center cell experienced little or no scattering in passing through the neon layer between the fuel and the wall, while the neutrons entering the center cell transparent wall from the six outer unit cells pass through a layer of BeO. It would be expected, therefore, that the fast neutron spectrum seen by the transparent wall would be similar to that calculated for a point isotropic fission source in an infinite medium of beryllium. The fast neutron flux at the transparent wall at the midplane of the center unit cell calculated by the QADHD code was essentially equal to that resulting from the one-dimensional, 24-group neutron transport-theory calculations.

The calculated gamma heating rates and dose rates and total heat and doses received in the transparent-wall material of the full-scale engine are presented in Table XI. The total gamma radiation which could be expected to direct itself toward the transparent

wall in the center cell should be 4/7 of the total gamma energy emission, 1/7 coming from inside the central cell plus 3/7 coming from the six external unit cells. The mean buildup factors for the gamma radiation arriving at the transparent wall of the center cell are rather low. This is to be expected because the BeO between the center cell and the external cells is relatively thin; the radiation from the center cell passing through the internal transparent wall needs to penetrate only the very diffuse neon between the fuel region and the transparent wall. The particular location of the transparent wall chosen should be exposed to the maximum gamma energy flux.

Comparisons of the radiation environment in the nuclear light bulb and the Union Carbide and TRIGA test reactors are presented in Table XII. The main points of interest are the comparisons of total neutron and gamma heat depositions and the comparisons of the ratios of gamma to neutron heat deposition in the different radiation environments. The total heat deposition in the engine during a 1000-sec operating time is of the same order of magnitude as that experienced in the Union Carbide test reactor. However, there are two major differences. First, the ratio of gamma to neutron heat deposition in the engine is approximately 9.3. The same ratio for the Union Carbide test reactor is about 20. There are three causes for this difference. First, the gamma energy release in the Union Carbide test reactor is from fission fragments in equilibrium whereas in the engine the fission fragments are present for only 20 sec, thus making the gamma energy release in the Union Carbide reactor higher by 5.2 mev per fission, an increase of about 50% above the 8.7 mev per fission release in the engine. This factor alone does not account for the difference in the ratio of gamma to neutron heating, however. Another factor of considerable importance is that the spectrum of fast neutrons in the Union Carbide test reactor is quite different since it is the spectrum in light water rather than beryllium. Calculations using the different spectra have indicated that the effect of a light water spectrum would reduce the heating dose due to fast neutrons to about 80% of that which would result using a beryllium spectrum. These two factors still do not account for the difference in the two ratios. The final factor must be related to the distance between fuel elements and the location of the test sample, i.e., the amount of light water in the intervening space in the Union Carbide test reactor. Just a few inches of light water would remove a great many of the fast neutrons created by fission events in the fuel element. Gamma rays in this same environment have far greater penetrating powers and, therefore, are not degraded to such a large degree as the fast neutrons. Comparison with the TRIGA reactor indicates that the ratio of total gamma to total neutron energy deposition is 160 as compared to 20 in the Union Carbide reactor and 9.3 in the full-scale nuclear light bulb engine. An explanation for these differences is that the experimental location for the sample in the TRIGA reactor was in a beam port further away from an active fuel element than in the case of the Union Carbide reactor in which the sample was placed within the fuel element matrix. This would account for an even lower relative neutron dose rate at the sample location.

Dosages in the Filament-Wound Fiberglas Pressure Vessel

Studies of fiber-wound pressure vessels reported in Ref. 1 indicated that the nuclear radiation levels in the pressure vessel of a nuclear light bulb engine could potentially degrade the strength of a fiberglas laminate.

Results of neutron and gamma ray dose rate calculations for the pressure vessel are shown in Table XIII. The upper pressure vessel is protected from both neutron and gamma rays principally by the wide heat exchanger region containing both heavy metals and pressurized hydrogen gas at 2000 R. On the other hand, the lower pressure vessel is not nearly as well protected due to the penetrations through the end-wall moderator materials by the thrust nozzles (see Fig. 3). Therefore, there are large differences between the average and peak dose rates in the two end-wall pressure vessel segments as well as large differences in the ratio of peak-to-average dose rates.

The average dose rate for the entire filament-wound fiberglas pressure vessel was calculated to be 0.17 mrad/sec. This would allow about six full power runs of 1000-sec duration before the total dose became 1000 mrad, the estimated allowable dosage before degradation of the laminate strength commences. However, hot spots, particularly in the lower pressure vessel with dose rates as high as 3.69 mrad/sec were calculated. Further investigation is required to (1) verify more accurately for nuclear reactor radiation environments the threshold dosages which lead to laminate strength degradation and (2) to investigate the possibility of including a heat shield across the inner wall of the lower pressure vessel to reduce its radiation exposure.

Evaluation of Other Neutron and Gamma Ray Sources

There are other sources of neutrons and gamma rays to consider when estimating the total neutron and gamma heating rates and doses. These sources include (n, 2n), (γ, n), and (n,γ) reactions. Table XIV contains the candidate reactions considered and Table XV contains the calculated source strengths relative to the total neutron and gamma energy deposition rates by region. Secondary sources due to thermal neutron capture (n,γ) were calculated using the group-4 fluxes from two-dimensional diffusion theory calculations for the reference engine. The average cross-sections listed in Table XIV are for 2200 m/sec thermal neutrons. These cross-sections were adjusted in each region by the ratio of the average group-4 hydrogen absorption cross-section divided by the 2200 m/sec absorption cross-section for hydrogen. The (n, 2n) reaction ratios were calculated directly from the two-dimensional neutron diffusion theory results. Gamma fluxes used to calculate (γ, n) reaction rates were taken from the QADHD results for each region.

It can be seen from Table XV that the only secondary sources of substantial significance are those due to (n, γ) reactions in the pressure vessel which contribute a potential gamma source equal to about 16.5 percent of the energy deposition rate from fission sources. Although appreciable in absolute magnitude, the contribution by these (n, γ) reactions is not considered to be of enough significance to consider in detail for purposes of supplementing the fission neutron and gamma ray heating and dosages. It can be seen from Table XV that the magnitudes of the remaining secondary sources relative to those from fission neutrons and gamma rays are in all regions less than 5% of the total energy deposition rate by region.

Recommendations for Future Research

There are two principal areas in which further work is indicated. The sequence of cooling various engine components and the positioning of heat exhangers in the system should be rearranged to insure that the inlet temperature of the transparent wall coolant and other coolant inlet and outlet conditions throughout the system are maintained at the desired levels. In addition, a literature search should be conducted to determine the radiation dosage threshold in a reactor environment above which degradation of the strength of fiberglas laminates commences and calculations should be made of the thicknesses and weights of radiation shields which might be required to reduce dosages to the lower pressure vessel segment.

REFERENCES

1. McLafferty, G. H. and H. E. Bauer: Studies of Specific Nuclear Light Bulb and Open-Cycle Gaseous Nuclear Rocket Engines. United Aircraft Research Laboratories Report G-910093-37, prepared under Contract NASw-847, September 1967. Also issued as NASA CR-1030.

2. Latham, T. S.: Nuclear Criticality Studies of Specific Nuclear Light Bulb and Open-Cycle Gaseous Nuclear Rocket Engines. United Aircraft Research Laboratories Report F-910375-2, prepared under Contract NASw-847, September 1967.

3. Latham, T. S.: Heat Generation in Nuclear Fuel During Injection Into a Gaseous Nuclear Rocket Engine. AIAA Paper No. 66-620, presented at AIAA Second Propulsion Joint Specialist Conference, Colorado Springs, Colo., June 1966. Also issued as United Aircraft Research Laboratories Report UAR-E57, prepared under Contract NASw-847, April 1966.

4. Engle, W. W.: A Users Manual for ANISN, A One Dimensional Discrete Ordinates Transport Code with Anisotropic Scattering. Union Carbide Corporation Nuclear Division Report No. K-1693, March 30, 1967.

5. Fowler, T. B., M. L. Tobias, and D. R. Vondy: EXTERMINATOR-II: A Fortran IV Code for Solving Multigroup Neutron Diffusion Equations in Two Dimensions. Union Carbide Corporation, prepared for the U. S. Atomic Energy Commission, Report No. ORNL-4078, April 1967.

6. Mynatt, F. R.: A Users Manual for DOT, A Two Dimensional Discrete Ordinates Transport Code with Anisotropic Scattering. Union Carbide Corporation Nuclear Division Report K-1964 (In Publication).

7. Joanou, G. D. and J. S. Dudek: GAM-1, A Consistent P-1 Multigroup Code for the Calculation of Fast Neutron Spectra and Multigroup Constants. General Atomics Report GA-1850, June 1961.

8. Shudde, R. H. and J. Dyer: TEMPEST-II, A Neutron Thermalization Code. North American Aviation, Report No. AMTD-111, September 1960.

9. Canfield, E. H., R. N. Stuart, R. P. Freis, and W. H. Collins: SOPHIST-I, An IBM 709/7090 Code which Calculates Multigroup Transfer Coefficients for Gaseous Moderators. University of California Lawrence Radiation Laboratory Report UCRL-5956, Livermore, California, October 1961.

REFERENCES (Continued)

10. Latham, T. S.: Nuclear Criticality Study of a Specific Vortex-Stabilized Gaseous Nuclear Rocket Engine. United Aircraft Research Laboratories Report E-910375-1, October 1966. Also issued as NASA CR-697.

11. Kesten, A. S. and N. L. Krascella: Theoretical Investigation of Radiant Heat Transfer in the Fuel Region of a Gaseous Nuclear Rocket Engine. United Aircraft Research Laboratories Report E-910092-9, prepared under Contract NASw-847, September 1966. Also issued as NASA CR-695.

12. Stewart, J. C. and P. F. Zweifel: Proceedings of the Second International Conference on the Peaceful Uses of Atomic Energy. Vol. 16, United Nations, New York, 1958, p. 650.

13. MacPhee, J.: The Kinetics of Circulating Fuel Reactors. Nuclear Science and Engineering, Vol. 4, 1958, p. 588.

14. Keepin, R. G. and T. F. Wimett: Reactor Kinetics Functions: A New Evaluation. Nucleonics, Vol. 16, No. 10, 1958, p. 86.

15. Lahti, G. P.: QADHD, A Point Kernel Radiation Shielding Code to Calculate Dose Rates, Time Integrated Dose, and Propellant Heating. NASA-Lewis Research Center Report NASA TAX-1397, Cleveland, Ohio, November 30, 1965.

16. Kutcher, J. W. and M. E. Wyman: An Experimental Study of the Time Dependence of the Beta Energy Spectrum from U-233 Fission Fragments. Nuclear Science and Engineering, Vol. 26, 1966, p. 435.

17. Engle, L. B., P. C. Fisher, and M. P. Kellogg: Energy and Time Dependence of Delayed Gammas from Fission. Los Alamos Scientific Laboratory Report LAMS-2642, January 1962.

18. Anon.: Reactor Physics Constants. Argonne National Labortory Report ANL-5800, Second Edition, July 1963.

19. Krumbein, A. D.: Summary of NDA Unclassified Results of Moments Calculations for the Penetration of Neutrons Through Various Materials. Nuclear Development Corporation of America Report NDA-92-2 (Rev.) August 30, 1957.

20. Douglas, F. C., R. Gagosz, and M. A. DeCrescente: Optical Absorption in Transparent Materials Following High Temperature Reactor Irradiation. UARL Report F-910485-2, September 1967. Also issued as NASA CR-1031.

21. Gagosz, R., J. Waters, F. C. Douglas, and M. A. DeCrescente: Optical Absorption in Fused Silica During TRIGA Reactor Pulse Irradiations. UARL Report F-910485-1, September 1967. Also issued as NASA CR-1032.

22. Gagosz, R. M. and J. Waters: Optical Absorption and Fluorescence in Fused Silica During TRIGA Pulse Irradiation. UARL Report G-910485-3, April 1968.

23. Douglas, F. C. and R. M. Gagosz: Experimental Investigation of Thermal Annealing of Nuclear-Reactor-Induced Coloration in Fused Silica. UARL Report D-910082-7, March 1965. Also issued as NASA CR-304.

LIST OF SYMBOLS

A	Atomic mass number, dimensionless
A_T	Effective area of nozzle throat, ft^2
a	Step function coefficient, dimensionless
C_i	Delayed neutron precursor density, precursors/cm^2
c	Ramp function coefficient, sec^{-1}
$\overline{\cos\theta}$	Average neutron scattering angle in center-of-mass coordinate system
db	Decibels, $20 \log_{10}\left[(\Delta n/n_o)/(\Delta k/k)\right]$ or $20 \log_{10}\left[(\Delta n/n_o)/(\Delta\lambda_F/\lambda_{F_o})\right]$
E	Neutron energy, ev or Mev
E_i	Mean neutron energy for group i, Mev
f_{IM}	Internal moderation fraction (see text for description), dimensionless
f_{RM}	Radial moderator fraction, ratio of moderator mass in radial direction to total moderator mass, dimensionless
k_{eff}	Effective multiplication factor, dimensionless
ℓ^*	Prompt neutron lifetime, sec
$\bar{l}$	Mean first-flight track length, cm
M	Mass, lb
M_C	Critical mass, lb
n	Neutron level, neutrons/cm^3
P_I/P_O	Ratio of power per unit cavity between inner and outer cavities, dimensionless
P_c	Nominal chamber operating pressure, atm
R_f	Fuel region radius, cm

LIST OF SYMBOLS (Continued)

T	Absolute temperature, deg K or deg R
T_{MM}	Mixed mean propellant temperature, deg K or deg R
t	Time, sec
v	Neutron velocity, cm/sec
β	Delayed neutron fraction, dimensionless
β_i	Delayed neutron fraction in i^{th} group, dimensionless
$\Delta A_T/A_{T_o}$	Fractional change in effective area of nozzle throat, dimensionless
$\overline{\Delta E}$	Average energy degradation per neutron scattering collision, Mev
$\Delta k/k$ or $\delta k/k$	Fractional change in effective multiplication factor, dimensionless
$\Delta M/M_C$	Fractional change in fuel mass, dimensionless
$\Delta M_{HF}/M_{HF_o}$	Fractional change in hafnium mass, dimensionless
$\Delta M_W/M_{W_o}$	Fractional change in tungsten mass, dimensionless
$\Delta P_c/P_{c_o}$	Fractional change in nominal chamber operating pressure, dimensionless
$\Delta R_f/R_{f_o}$	Fractional change in fuel region radius, dimensionless
$\Delta T/T_o$	Fractional change in nominal operating temperature, dimensionless
$\Delta T_{MM}/T_{MM_o}$	Fractional change in mixed mean propellant temperature, dimensionless
δk	Reactivity, dimensionless
$\delta\lambda_F/\lambda_{F_o}$	Fractional change in fuel decay constant, dimensionless
λ_F	Fuel decay constant, sec^{-1}
λ_i	Decay constant for i^{th} delayed neutron precursor, sec^{-1}

LIST OF SYMBOLS (Continued)

μ_a	Gamma ray absorption coefficient, cm^{-1}
μ_{ij}	Probability for neutron energy transfer by scattering from neutron energy group i to j
ρ	Density, lb/ft^3 or gm/cm^3
Σ_s	Macroscopic scattering cross-section for neutrons, cm^{-1}
σ_a	Microscopic absorption cross-section, barns
σ_f	Microscopic fission cross-section, barns
σ_s	Microscopic scattering cross-section, barns
σ_{tr}	Microscopic transport cross-section, barns
τ_i	Mean lifetime of i^{th} delayed neutron precursor, sec
ω	Frequency, rad/sec
Subscript	
o	Denotes nominal operating condition
Superscript	
i	Denotes neutron energy group

TABLE I

COMPOSITIONS OF REGIONS EMPLOYED IN
ONE- AND TWO-DIMENSIONAL CALCULATIONS
FOR REFERENCE ENGINE

Geometry and Dimensions of
Regions Shown In Fig. 3

Region		Volume Fractions													
Description	No.	Ne 15,000 R	Ne 2000 R	SiO_2 2000 R	H_2 2000 R	H_2 12,000 R	H 12,000 R	H_2 4000 R	Al 1360 R	Be 1000 R	BeO 2529 R	C 4086 R	Hf 1000 R	SS 1000 R	W-nat 4000 R
Fuel*	5, 9	-	-	-	-	-	-	-	-	-	-	-	-	-	-
Hot Gases	6, 8, 10	0.1327	0.0572	0.0289	0.2031	0.2500	0.2355	0.0789	0.0002	0.0134	-	-	-	-	-
Inner BeO	7	-	0.0073	0.0422	0.2192	-	-	-	-	0.0183	0.6918	0.0194	-	-	-
Outer BeO	11	-	0.0025	0.0190	0.1267	-	-	-	-	0.0640	0.7802	0.0066	-	-	-
Upper BeO	4	-	0.0061	0.0071	0.0980	-	-	0.1611	0.0005	0.0137	0.6953	0.0056	0.0035	-	-
Lower BeO	14	-	0.0022	0.0171	0.1140	-	-	-	-	0.0576	0.7022	0.0059	-	-	-
Outer Graphite	12	-	-	-	-	-	-	0.0486	-	0.0011	-	0.9503	-	-	-
Upper Graphite	3	-	0.0061	0.0071	0.0980	-	-	0.1611	0.0005	0.0137	-	0.6909	0.0035	-	-
Lower Graphite	15	-	-	-	-	-	-	0.1437	-	0.0010	-	0.8554	-	-	-
Nozzles	13	-	-	-	-	0.5149	0.4851	-	-	-	-	-	-	-	-
Pressure Vessel**	1	-	-	-	-	-	-	-	-	-	-	-	-	-	-
Heat Exchanger	2	-	-	-	0.8700	-	-	-	-	-	-	-	-	0.1260	0.004

* Fuel region volume fractions in a mixture of U-233 and Ne were varied to achieve criticality with the constraint that the sum of the U-233 and Ne atom densities was equal to 9.0×10^{19} atoms/cm^3.

** Pressure vessel composition was as follows: Volume fraction of fiberglass and resin = 0.80
Volume fraction of internal hydrogen coolant (H_2 at 432 R, 250 atm) = 0.20
Composition of fiberglass and resin laminate by weight:
Resin, $C_6H_4(NH_2)_2$ = 24.0%, SiO_2 = 49.4%, Al_2O_3 = 19.0%, MgO = 7.6%

TABLE II

DENSITIES AND WEIGHTS OF MATERIALS EMPLOYED IN REFERENCE ENGINE CRITICALITY CALCULATIONS

Dimensions and Geometry of Regions Given in Fig. 3
Composition of Regions Given in Table I

Material	Mass Density - lb/ft^3	Total Mass in all Regions - lb
Neon, 15,000 R	0.9435	14.8
Neon, 2000 R	6.9260	52.6
Silicon dioxide, 2000 R	157.30	890.0
Hydrogen, 12,000 R	0.0749	16.0
Hydrogen, 4000 R	0.3420	14.6
Hydrogen, 2000 R	0.686	99.7
Aluminum, 1360 R	168.48	12.5
Beryllium, 1000 R	114.82	764.0
Beryllium Oxide, 2529 R	178.20	12200.0
Graphite, 4068 R	114.82	26800.0
Hafnium, 1000 R	823.70	131.6
Pressure Vessel, 432 R	122.00	23400.0
Stainless Steel, 1000 R	500.40	7394.0
Tungsten, 4068 R	1173.0	550.0
Hydrogen, 432 R	1.3678	67.9
	TOTAL*	72407.7

*See Text (Note: not equal to weight in Ref. 1)

TABLE III

NEUTRON ENERGY GROUP STRUCTURES USED IN CRITICALITY CALCULATIONS

Neutron Energy Group	Upper Energy Limit, ev	Lower Energy Limit, ev	Group Number for Four-Group Structure Used For Nuclear Light Bulb Engine
1	1.0×10^7	2.865×10^6	
2	2.865×10^6	1.35×10^6	
3	1.35×10^6	8.21×10^5	1
4	8.21×10^5	3.88×10^5	
5	3.88×10^5	1.11×10^5	
6	1.11×10^5	1.50×10^4	2
7	1.50×10^4	3.35×10^3	
8	3.35×10^3	5.83×10^2	
9	5.83×10^2	1.01×10^2	
10	1.01×10^2	29.0	3
11	29.0	8.32	
12	8.32	3.06	
13	3.06	2.38	
14	2.38	1.86	
15	1.86	1.44	
16	1.44	1.125	
17	1.125	0.685	4
18	0.685	0.414	
19	0.414	0.3	
20	0.3	0.2	
21	0.2	0.1	
22	0.1	0.05	
23	0.05	0.015	
24	0.015	0.0	

TABLE IV

TABLE OF REACTIVITY COEFFICIENTS
FOR REFERENCE ENGINE

Material or Region	Reactivity Coefficient	Numerical Value
U-233	$(\Delta k/k)/(\Delta M/M_C)$	+0.3840
Neon & Hydrogen Gases, All Regions	$(\Delta k/k)/(\Delta P_c/P_{c_o})$	+0.0859
All Regions	$(\Delta k/k)/(\Delta T/T_o)$	+0.0450
Hydrogen Gases In Propellant Region	$(\Delta k/k)/(\Delta T_{MM}/T_{MM_o})$	+0.0544
Fuel Region	$(\Delta k/k)/(\Delta R_F/R_{F_o})$	-0.0413
Hafnium In Upper End Walls	$(\Delta k/k)/(\Delta M_{Hf}/M_{Hf_o})$	-0.01346
Tungsten In Propellant Gases	$(\Delta k/k)/(\Delta M_W/M_{W_o})$	-2.31×10^{-5}
Tungsten In Nozzle Gases	$(\Delta k/k)/(\Delta M_W/M_{W_o})$	-6.30×10^{-7}

TABLE V

DELAYED NEUTRON YIELDS FOR U-233

Total Delayed Neutron Fraction, $\beta = 0.0025$

Mean Life, τ_i sec	Decay Constant, λ_i sec^{-1}	Yield Fraction, β_i
0.321	3.12	0.000061
0.788	1.27	0.000194
3.300	0.303	0.000845
7.650	0.131	0.000604
29.900	0.0335	0.000730
79.500	0.0126	0.000024

TABLE VI

GAMMA RAY SPECTRUM USED FOR HEATING AND DOSE CALCULATIONS

Gamma Energy Group	Mean Energy, Mev	Energy Group Limits, Mev	Prompt Gamma Energy Spectrum, Mev/Fission	Normalized Gamma* Energy Spectrum, Mev/Fission
1	0.5	0.0-0.75	1.550	1.720
2	1.0	0.75-1.25	1.900	2.100
3	1.5	1.25-1.75	1.260	1.400
4	2.0	1.75-2.25	1.100	1.220
5	2.5	2.25-2.75	0.725	0.805
6	3.0	2.75-3.25	0.450	0.500
7	3.5	3.25-3.75	0.217	0.241
8	4.0	3.75-4.25	0.260	0.289
9	4.5	4.25-4.75	0.108	0.120
10	5.0	4.75-5.25	0.095	0.106
11	5.5	5.25-5.75	0.094	0.105
12	6.0	5.75-6.25	0.042	0.047
13	6.5	6.25-10.0	0.026	0.029

* Normalization accounts for a total prompt gamma energy release of 7.2 Mev plus the release of 1.5 Mev delayed gamma energy during 20 sec after fission (see Fig. 22).

TABLE VII

PRODUCT OF NEUTRON ELASTIC SCATTERING CROSS-SECTIONS AND AVERAGE ENERGY DEGRADATION FOR ENGINE MATERIALS

$$\overline{\Delta E} = E\left[2A/(1+A)^2\right](1-\overline{\cos\theta})$$

Σ_S calculated using the GAM-I Code, Ref. 7

$\overline{\Delta E}\Sigma_S$ for a specified material = $\sum_j (\overline{\Delta E}\Sigma_S)_j$,

where j denotes atomic constituents of material molecule.

Material densities and compositions given in Tables I and II.

Neutron Energy Group	Energy Group Limits, Mev	Mean Energy, Mev	$\overline{\Delta E}\Sigma_S$ For Specified Material, Mev/cm										
			SiO_2	Al	Stainless Steel	BeO	C	Resin	Fiber-glas	W	Hf	Be	H*
1	12.0-9.0	10.00	0.08910	0.03797	0.06133	0.25540	0.10660	0.56300	0.08004	0.01692	0.02037	0.24770	0.03139
2	9.0-7.0	8.00	0.03526	0.03026	0.04917	0.15240	0.08266	0.46850	0.03176	0.01355	0.01629	0.19790	0.02508
3	7.0-5.5	6.0	0.03531	0.01029	0.04224	0.13190	0.07000	0.37410	0.03001	0.01122	0.01352	0.15910	0.02195
4	5.5-4.5	5.00	0.05165	0.01067	0.03811	0.13510	0.07067	0.39990	0.04434	0.01049	0.01265	0.13070	0.02210
5	4.5-3.5	4.00	0.05558	0.02767	0.02924	0.14660	0.10540	0.41210	0.04985	0.00912	0.01098	0.13560	0.02129
6	3.5-2.5	3.00	0.03214	0.02960	0.02087	0.12440	0.08175	0.39040	0.02862	0.00747	0.00900	0.15740	0.02054
7	2.5-1.5	2.00	0.03524	0.02326	0.01511	0.08467	0.06202	0.33560	0.01068	0.00516	0.00622	0.08282	0.01599
8	1.5-0.835	1.00	0.03072	0.01388	0.00856	0.07718	0.03288	0.21040	0.02709	0.00288	0.00346	0.07150	0.01061
9	0.835-0.5	0.67	0.01638	0.00961	0.00711	0.03607	0.02767	0.18010	0.01440	0.00260	0.00312	0.03150	0.00908
10	0.5-0.1	0.33	0.01145	0.00583	0.00516	0.03086	0.01752	0.16120	0.01011	0.00176	0.00212	0.03150	0.00606

* Hydrogen at 4000 R and 500 atm.

TABLE VIII

GAMMA RAY ENERGY ABSORPTION COEFFICIENTS FOR ENGINE MATERIALS

$\mu_a = \rho \left[\mu_a / \rho \right]$ - cm^{-1}

$\left[\mu_a / \rho \right]$ taken from Ref. 18.

Material densities and compositions given in Tables I and II

Gamma Energy Group	Energy Group Limits, Mev	Mean Energy, Mev	Energy Absorption Coefficients for Specified Material, μ_a - cm^{-1}										
			SiO_2	Al	Stainless Steel	BeO	C	Resin	Fiber-glas	W	Hf	Be	H*
1	0.0-0.75	0.5	0.07420	0.07720	0.26000	0.08850	0.05460	0.01500	0.04320	1.47800	1.03800	0.04860	0.000650
2	0.75-1.25	1.0	0.06950	0.07290	0.23100	0.08050	0.05150	0.01410	0.04070	0.66400	0.46600	0.04560	0.000613
3	1.25-1.75	1.5	0.06400	0.06700	0.21400	0.07380	0.04710	0.01290	0.03740	0.52800	0.37100	0.04180	0.000560
4	1.75-2.25	2.0	0.05970	0.06260	0.20400	0.06840	0.04360	0.01190	0.03480	0.50900	0.35800	0.03860	0.000514
5	2.25-2.75	2.5	0.05620	0.05490	0.20000	0.06440	0.04100	0.01120	0.03320	0.52500	0.36800	0.03610	0.000477
6	2.75-3.25	3.0	0.05390	0.05720	0.19600	0.06050	0.03850	0.01050	0.03150	0.54000	0.37900	0.03370	0.000441
7	3.25-3.75	3.5	0.05200	0.05560	0.19600	0.05800	0.03680	0.01000	0.03050	0.56200	0.39500	0.03200	0.000416
8	3.75-4.25	4.0	0.05040	0.05400	0.19500	0.05510	0.03500	0.00953	0.02940	0.58500	0.41100	0.03020	0.000389
9	4.25-4.75	4.5	0.04900	0.05290	0.19600	0.05330	0.03130	0.00876	0.02870	0.60700	0.42600	0.02890	0.000370
10	4.75-5.25	5.0	0.04800	0.05180	0.19700	0.05140	0.03260	0.00885	0.02790	0.63000	0.44200	0.02780	0.000350
11	5.25-5.75	5.5	0.04710	0.05130	0.19800	0.05020	0.03160	0.00862	0.02750	0.64900	0.45500	0.02690	0.000345
12	5.75-6.25	6.0	0.04630	0.05080	0.20000	0.04880	0.03050	0.00830	0.02700	0.66700	0.46900	0.02590	0.000320
13	6.25-10.0	6.5	0.04570	0.05050	0.20100	0.04790	0.03000	0.00813	0.02660	0.68400	0.48000	0.02540	0.000309

TABLE IX

NEUTRON, GAMMA RAY, AND TOTAL HEATING BY REGION IN NUCLEAR LIGHT BULB ENGINE FOR DIFFERENT AVERAGE FUEL RESIDENCE TIMES

Total Power = 4600 megw = 1.5×10^{20} Fissions/sec = 4.37×10^{6} Btu/sec
Gamma Ray and Beta Particle Energy Release as a Function of Time after Fission of U-233 Shown in Fig. 22
Geometry and Composition of Regions Given in Tables I and II and in Fig. 3

Region		Heat Deposition Rate, megw								
		Average Fuel Residence Time = 1.0 sec			Average Fuel Residence Time = 20.0 sec			Average Fuel Residence Time = 60.0 sec		
Description	Number	Neutron	Gamma	Total	Neutron	Gamma	Total	Neutron	Gamma	Total
Pressure Vessel	1	7.91	8.14	16.05	7.91	9.46	17.37	7.91	10.23	18.14
Heat Exchanger	2	0.02	0.40	0.42	0.02	0.46	0.48	0.02	0.50	0.52
Upper Graphite	3	0.36	1.98	2.35	0.36	2.31	2.67	0.36	2.49	2.85
Upper BeO	4	2.61	15.87	18.48	2.61	18.44	21.05	2.61	19.95	22.56
Transparent Walls, Neon, Cavity Liner	6,8,10	2.31	11.93	14.24	2.31	13.88	16.19	2.310	15.100	17.41
Inner BeO	7	8.89	26.33	35.22	8.89	30.60	39.49	8.89	33.10	41.99
Outer BeO	11	15.11	31.34	46.45	15.11	36.42	51.53	15.11	39.40	54.51
Outer Graphite	12	10.73	33.37	44.10	10.73	38.78	49.51	10.73	41.95	52.68
Nozzles	13	0.08	--	0.08	0.08	--	0.08	0.08	--	0.08
Lower BeO	14	4.99	20.88	25.87	4.99	24.26	29.25	4.99	26.24	31.23
Lower Graphite	15	4.09	11.18	15.27	4.09	12.99	17.08	4.09	14.05	18.14
Sub-Total				218.53			244.70			260.11
Leakage	--	6.20	13.20	19.40	6.20	15.32	21.52	6.20	16.57	22.77
Heat Exchanger*	2	--	--	268.00	--	--	143.50	--	--	110.50
Fuel**	5,9	--	--	4036.00	--	--	4131.60	--	--	4147.60
Hydrogen Propellant Between Fuel and Cavity Walls	6,8,10	54.33	3.74	58.07	54.33	4.35	58.68	54.33	4.69	59.02
TOTAL				4600.0			4600.00			4600.00

* Delayed gamma and beta energy deposited in fuel separation and recirculation system.

** Fission fragment and beta energy deposited in active core.

TABLE X

NEUTRON HEATING AND DOSE RATES IN TRANSPARENT WALL

Total Power = 4600 megw = 1.50×10^{20} Fissions/sec = 2.88×10^{22} Mev/sec

Neturon Energy Group	Mean Energy, Mev	Energy Group Limits, Mev	Neutron Flux, neutron/cm^2-sec	Energy Flux, Mev/cm^2-sec	Heating Rate In SiO_2, Mev/cm^3-sec	Dose Rate In SiO_2, Rad/sec
1	10.0	12.0-9.0	4.84×10^{13}	4.84×10^{14}	4.32×10^{12}	2.74×10^{4}
2	8.0	9.0-7.0	1.91×10^{14}	1.53×10^{15}	6.73×10^{12}	4.27×10^{4}
3	6.0	7.0-5.5	8.13×10^{13}	$4,88 \times 10^{14}$	2.87×10^{12}	1.82×10^{4}
4	5.0	5.5-4.5	7.52×10^{13}	3.76×10^{14}	3.88×10^{12}	2.46×10^{4}
5	4.0	4.5-3.5	1.67×10^{14}	6.67×10^{14}	9.28×10^{12}	5.89×10^{4}
6	3.0	3.5-2.5	3.19×10^{14}	9.55×10^{14}	1.03×10^{13}	6.54×10^{4}
7	2.0	2.5-1.5	5.73×10^{14}	1.15×10^{15}	2.02×10^{13}	1.28×10^{5}
8	1.0	1.5-0.835	6.38×10^{14}	6.38×10^{14}	1.96×10^{13}	1.24×10^{5}
9	0.67	0.835-0.5	5.69×10^{14}	3.82×10^{14}	9.33×10^{12}	5.92×10^{4}
10	0.33	0.5-0.1	3.64×10^{14}	1.20×10^{14}	4.17×10^{12}	2.65×10^{4}
		TOTALS	3.02×10^{15}	6.79×10^{15}	9.07×10^{13}	5.75×10^{5}

Conversion Factor: (Mev/cm^3-sec) $\times 0.635 \times 10^{-8}$ = Rad/sec in SiO_2

TABLE XI

GAMMA RAY HEATING AND DOSE RATES IN TRANSPARENT WALL

Total Power = 4600 megw = 1.50×10^{20} Fission/sec = 2.88×10^{22} Mev/sec

Gamma Energy Group	Mean Energy, Mev	Energy Group Limits, Mev	Direct Beam Energy Flux, Mev/cm^2-sec	Mean Buildup Factors	Heating Rate In SiO_2 Direct Beam, Mev/cm^3-sec	Heating Rate In SiO_2 With Buildup, Mev/cm^3-sec	Dose Rate In SiO_2 Direct Beam, Rad/sec	Dose Rate In SiO_2 With Buildup, Rad/sec
1	0.5	0.0-0.75	2.23×10^{15}	1.180	1.65×10^{14}	1.94×10^{14}	1.05×10^{6}	1.23×10^{6}
2	1.0	0.75-1.25	2.92×10^{15}	1.098	2.02×10^{14}	2.23×10^{14}	1.28×10^{6}	1.42×10^{6}
3	1.5	1.25-1.75	1.99×10^{15}	1.073	1.27×10^{14}	1.36×10^{14}	8.06×10^{5}	8.64×10^{5}
4	2.0	1.75-2.25	1.75×10^{15}	1.058	1.05×10^{14}	1.11×10^{14}	6.67×10^{5}	7.05×10^{5}
5	2.5	2.25-2.75	1.16×10^{15}	1.049	6.53×10^{13}	6.82×10^{13}	4.15×10^{5}	4.33×10^{5}
6	3.0	2.75-3.25	7.23×10^{14}	1.042	3.91×10^{13}	4.07×10^{13}	2.48×10^{5}	2.58×10^{5}
7	3.5	3.25-3.75	3.50×10^{14}	1.037	1.82×10^{13}	1.89×10^{13}	1.16×10^{5}	1.20×10^{5}
8	4.0	3.75-4.25	4.21×10^{14}	1.033	2.13×10^{13}	2.19×10^{13}	1.35×10^{5}	1.39×10^{5}
9	4.5	4.25-4.75	1.76×10^{14}	1.031	8.58×10^{12}	8.85×10^{12}	5.45×10^{4}	5.62×10^{4}
10	5.0	4.75-5.25	1.55×10^{14}	1.028	7.43×10^{12}	7.63×10^{12}	4.72×10^{4}	4.85×10^{4}
11	5.5	5.25-5.75	1.54×10^{14}	1.027	7.22×10^{12}	7.43×10^{12}	4.58×10^{4}	4.72×10^{4}
12	6.0	5.75-6.25	6.89×10^{13}	1.025	3.17×10^{12}	3.28×10^{12}	2.03×10^{3}	2.08×10^{3}
13	6.5	6.25-10.0	4.25×10^{13}	1.024	1.98×10^{12}	1.99×10^{12}	1.23×10^{3}	1.26×10^{3}
		TOTALS	1.21×10^{16}	1.095*	7.70×10^{14}	8.44×10^{14}	4.89×10^{6}	5.36×10^{6}

Conversion Factor: (Mev/cm^3-sec) x 0.635×10^{-8} = Rad/sec in SiO_2

*Average Value.

TABLE XII

COMPARISON OF TRANSPARENT WALL FLUXES, DOSE RATES, AND DOSAGES FOR NUCLEAR LIGHT BULB AND TEST REACTOR CONDITIONS

Reactor	Operating Time, Sec	Fast Neutron Flux, neutron/cm^2-sec	Fast Neutron Dose Rate, Rad/hr	Fast Neutron Heating Rate, Mev/cm^3-sec	Fast Neutron Heat Deposition, Mev/cm^3
Nuclear Light Bulb	10^3	3.02×10^{15}	2.08×10^9	9.07×10^{13}	9.07×10^{16}
Union Carbide Test Reactor (Core)	3.6×10^5	1.90×10^{13}	1.03×10^7	4.50×10^{11}*	1.60×10^{17}
Triga (Beam Port)	0.03	3.0×10^{15}	1.62×10^9	7.08×10^{13}*	2.12×10^{12}

Reactor	Gamma Dose Rate, Rad/hr	Gamma Heating Rate, Mev/cm^3-sec	Gamma Heat Deposition, Mev/cm^3-sec	Total Neutron and Gamma Dose Rate, Rad/hr	Total Neutron and Gamma Heat Deposition, Mev/cm^3
Nuclear Light Bulb	1.93×10^{10}	8.44×10^{14}	8.44×10^{17}	2.14×10^{10}	9.35×10^{17}
Union Carbide Test Reactor (Core)	2.00×10^8	9.00×10^{12}	3.20×10^{18}	2.10×10^8	3.36×10^{18}
Triga (Beam Port)	2.60×10^{11}	1.14×10^{16}	3.40×10^{14}	2.62×10^{11}	3.42×10^{14}

*Ratio of fast neutron heating rate to fast neutron flux different from that for Nuclear Light Bulb to correct for differences between Be and H_2O infinite media spectra.

Conversion Factors: (Mev/cm^3-sec) x 1.6×10^{-13} = watts/cm^3
(Watts/cm^3) x 27.85 = Btu/ft^3-sec
(Mev/cm^3-sec) x 0.229×10^{-4} = Rad/hr

TABLE XIII

NEUTRON, GAMMA RAY, AND TOTAL DOSE RATES IN FIBER-WOUND PRESSURE VESSEL

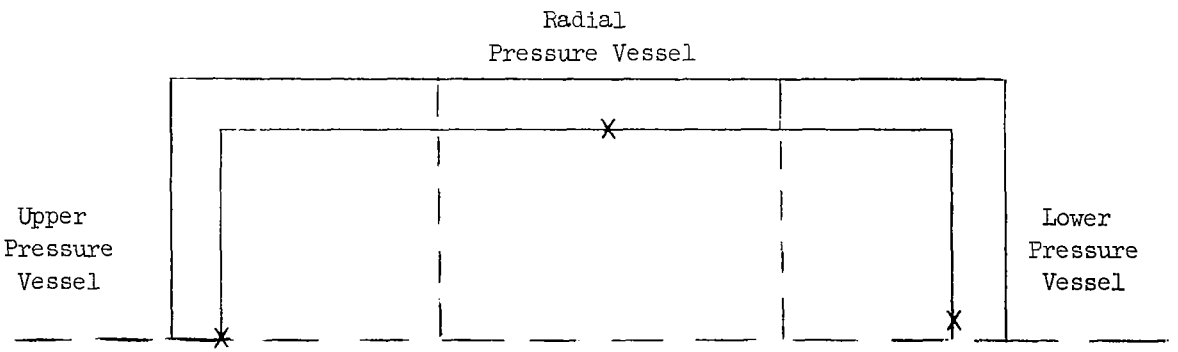

Pressure Vessel Region	Dose Rates, Rad/sec					
	Neutron		Gamma Ray		Total	
	Average*	Peak-to-Ave.** Ratio	Average*	Peak-to-Ave.** Ratio	Average*	Peak-to-Ave.** Ratio
Upper Pressure Vessel	475	9.37	510	2.84	985	8.31
Lower Pressure Vessel	263,000	7.05	363,000	1.44	626,000	5.88
Radial Pressure Vessel	45,900	9.40	47,350	2.50	93,250	7.63

* Averaged over entire volume of specified pressure vessel region

** Peaks occur at points on diagram denoted by X.

TABLE XIV

REACTIONS YIELDING SECONDARY NEUTRON AND GAMMA RAY SOURCES

Reaction Cross Sections and Mean Energies taken from Ref. 18

Material	Isotopic Abundance, Percent	Reaction	Average Cross Section, Barns	Mean Gamma or Neutron Energy Per Reaction, Mev	Gamma Ray Yield Per Thermal Neutron Capture, Percent
Be-9	100.0	(n, 2n)*	0.30	1.00	---
Be-9	100.0	(γ, n)**	0.001	0.90	---
N-15	0.37	(n, γ)	2.40×10^{-5}	6.37	75.0
O-18	0.20	(n, γ)	0.021	1.40	70.0
Ne-22	8.80	(n, γ)	0.036	0.48	30.0
Mg-26	11.30	(n, γ)	0.026	0.88	100.0
Al-27	100.00	(n, γ)	0.210	1.78	100.0
Si-30	3.12	(n, γ)	0.110	1.26	0.07
Cr-50	4.31	(n, γ)	13.50	0.32	100.0
Fe-58	0.31	(n, γ)	0.900	1.15	103.0
Ni-64	1.16	(n, γ)	1.60	1.25	47.1
Mo-92	15.86	(n, γ)	0.006	0.81	300.0
Mo-98	23.75	(n, γ)	0.450	0.47	26.0
Mo-100	9.62	(n, γ)	0.200	0.39	201.5
Hf-180	35.25	(n, γ)	10.0	0.29	213.5
W-180	0.135	(n, γ)	10.0	0.15	0.29
W-184	30.6	(n, γ)	2.10	1.48	200.0
W-186	28.4	(n, γ)	34.0	0.44	31.0

* Energy threshold for (n, 2n) reaction = 2.5 Mev

** Energy threshold for (γ, n) reaction = 1.7 Mev

TABLE XV

COMPARISON OF SECONDARY NEUTRON AND GAMMA RAY SOURCES TO TOTAL ENERGY DEPOSITION RATES BY REGION

Total Energy Deposition Rates Taken From Table IX For
Average Fuel Residence Time = 20.0 Sec
Secondary Source Strengths < 0.001 megw Ignored
Secondary Source Reaction Described in Table XIV

Region		Secondary Source Parent Isotope and Reaction	Secondary Source Strength, megw	Ratio of Secondary Source Strength to Total Energy Deposition Rate, Dimensionless
Description	No.			
Inner BeO	7	Be-9 (n, 2n)	0.632	
		Be-9 (γ, n)	0.002	
		O-18 (n, γ)	0.476	
		Sub-Total	1.110	0.0281
Hot Gases	6,8,10	Be-9 (n, 2n)	0.116	
		O-18 (n, γ)	0.041	
		Ne-22 (n, γ)	0.002	
		Al-27 (n, γ)	0.007	
		Sub-Total	0.166	0.0022
Outer BeO	11	Be-9 (n, 2n)	1.036	
		Be-9 (γ, n)	0.002	
		O-18 (n, γ)	0.958	
		Sub-Total	1.996	0.0387
Lower BeO	14	Be-9 (n, 2n)	0.558	
		Be-9 (γ, n)	0.001	
		O-18 (n, γ)	0.677	
		Sub-Total	1.236	0.0422
Upper BeO	4	Be-9 (n, 2n)	0.361	
		Be-9 (γ, n)	0.001	
		O-18 (n, γ)	0.684	
		Al-27 (n, γ)	0.007	
		Sub-Total	1.053	0.0500

TABLE XV (Continued)

Region		Secondary Source Parent Isotope and Reaction	Secondary Source Strength, megw	Ratio of Secondary Source Strength to Total Energy Deposition Rate, Dimensionless
Description	No.			
Upper Graphite	3	O-18 (n, γ)	0.004	
		Sub-Total	0.004	0.0015
Heat Exchanger	2	Fe-58 (n, γ)	0.001	
		Ni-64((n, γ)	0.026	
		Mo-100 (n, γ)	0.006	
		W-184 (n, γ)	0.462	
		W-186 (n, γ)	0.003	
		Sub-Total	0.498	0.0035
Pressure Vessel	1	Ni-15 (n, γ)	0.590	
		O-18 (n, γ)	0.697	
		Mg-26 (n, γ)	0.035	
		Al-27 (n, γ)	1.562	
		Sub-Total	2.874	0.1650
		TOTAL	8.927	0.0200

SCHEMATIC DIAGRAM OF REFERENCE NUCLEAR LIGHT BULB ENGINE

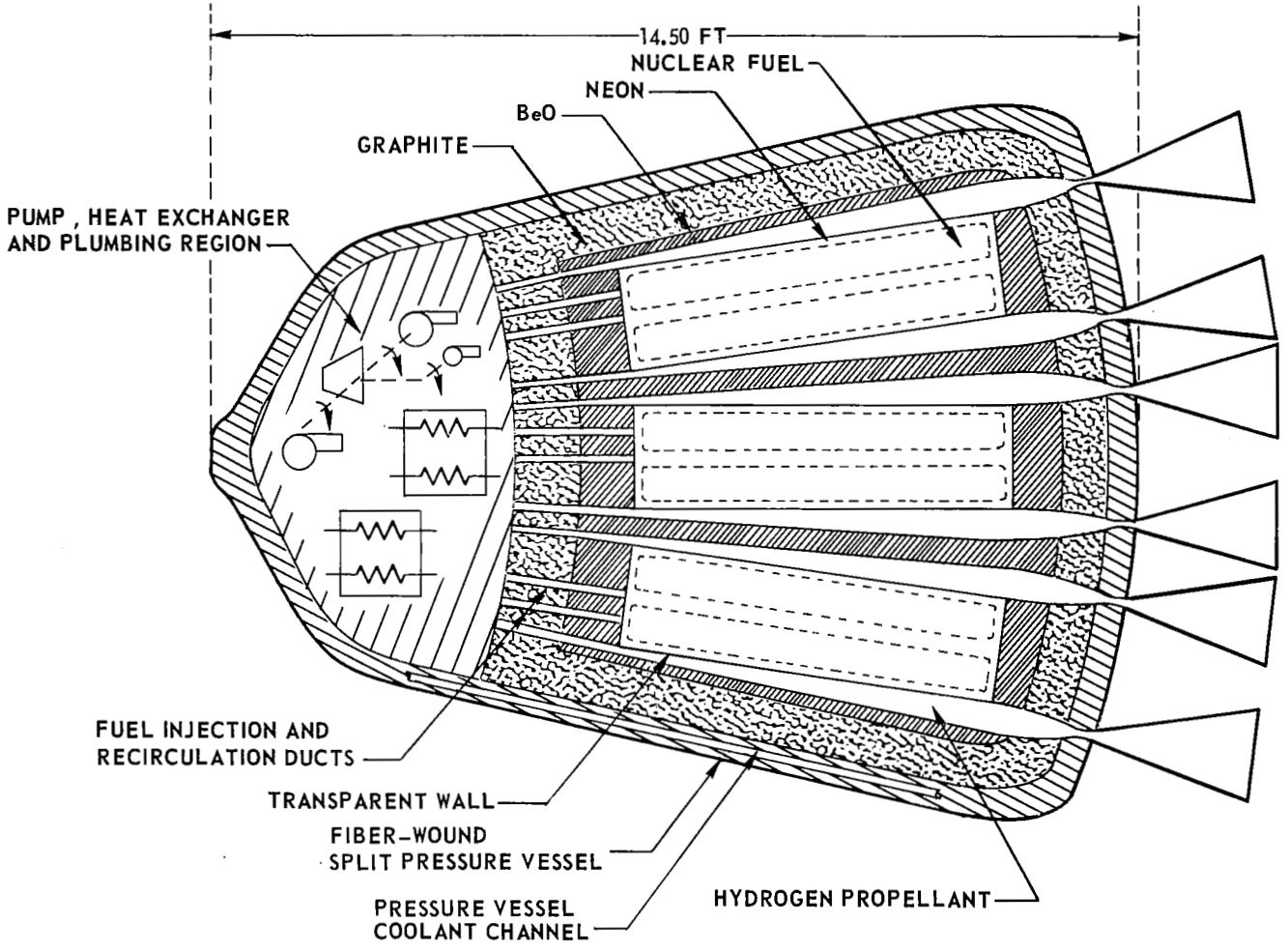

FIG. 1

FIG. 2

SECTOR OF REFERENCE NUCLEAR LIGHT BULB ENGINE CONFIGURATION

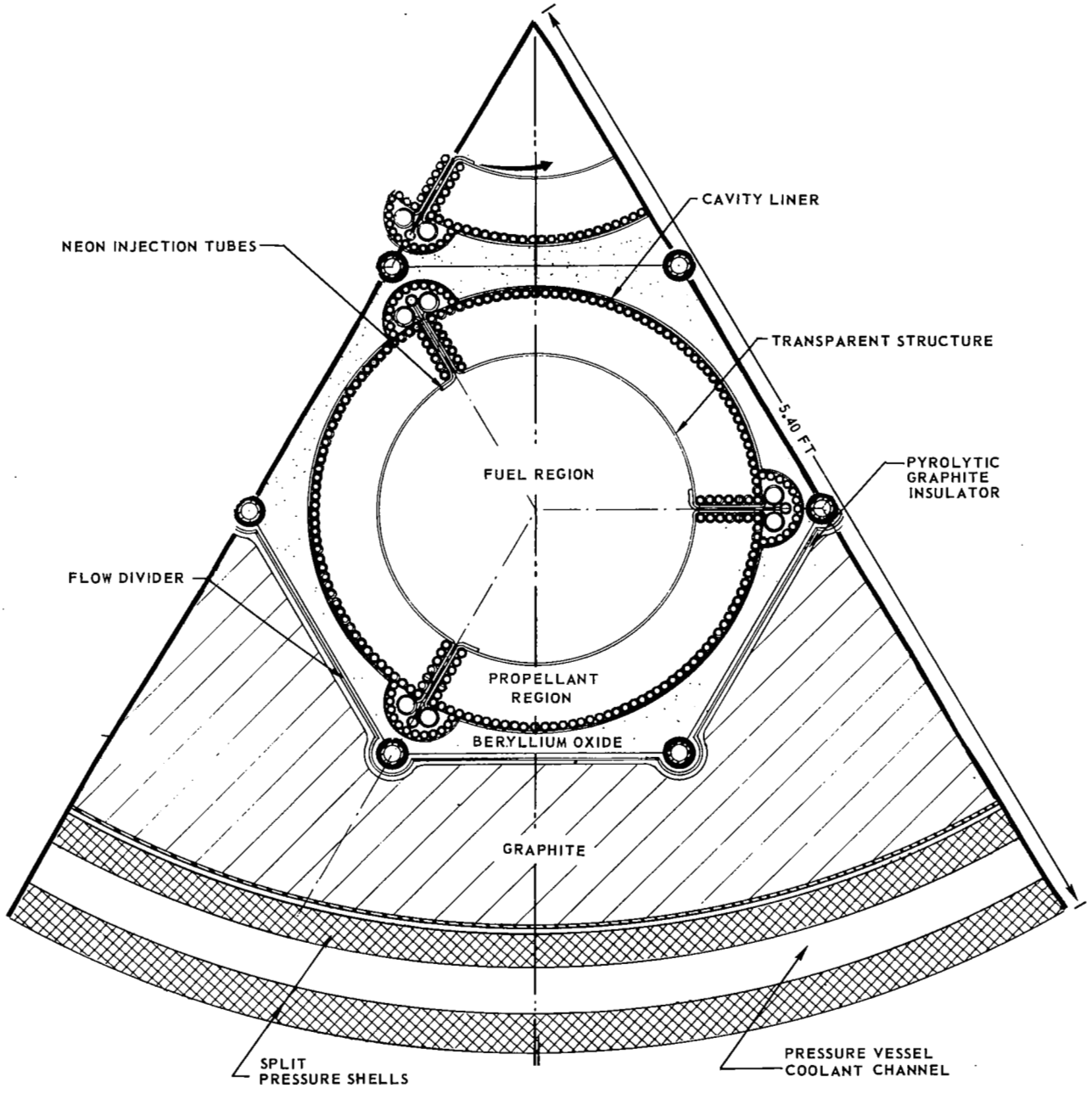

BASIC CYLINDRICAL GEOMETRY USED FOR ONE- AND TWO-DIMENSIONAL NUCLEAR LIGHT BULB CRITICALITY CALCULATIONS

CIRCLED NUMBERS INDICATE REGIONS DESCRIBED IN TABLE I

TOTAL WEIGHTS OF MATERIALS EMPLOYED GIVEN IN TABLE II

ONE-DIMENSIONAL GEOMETRY FROM RADIAL CROSS SECTION AT AXIAL MID-PLANE

UNCIRCLED NUMBERS INDICATE RADIAL AND AXIAL DIMENSIONS IN CM

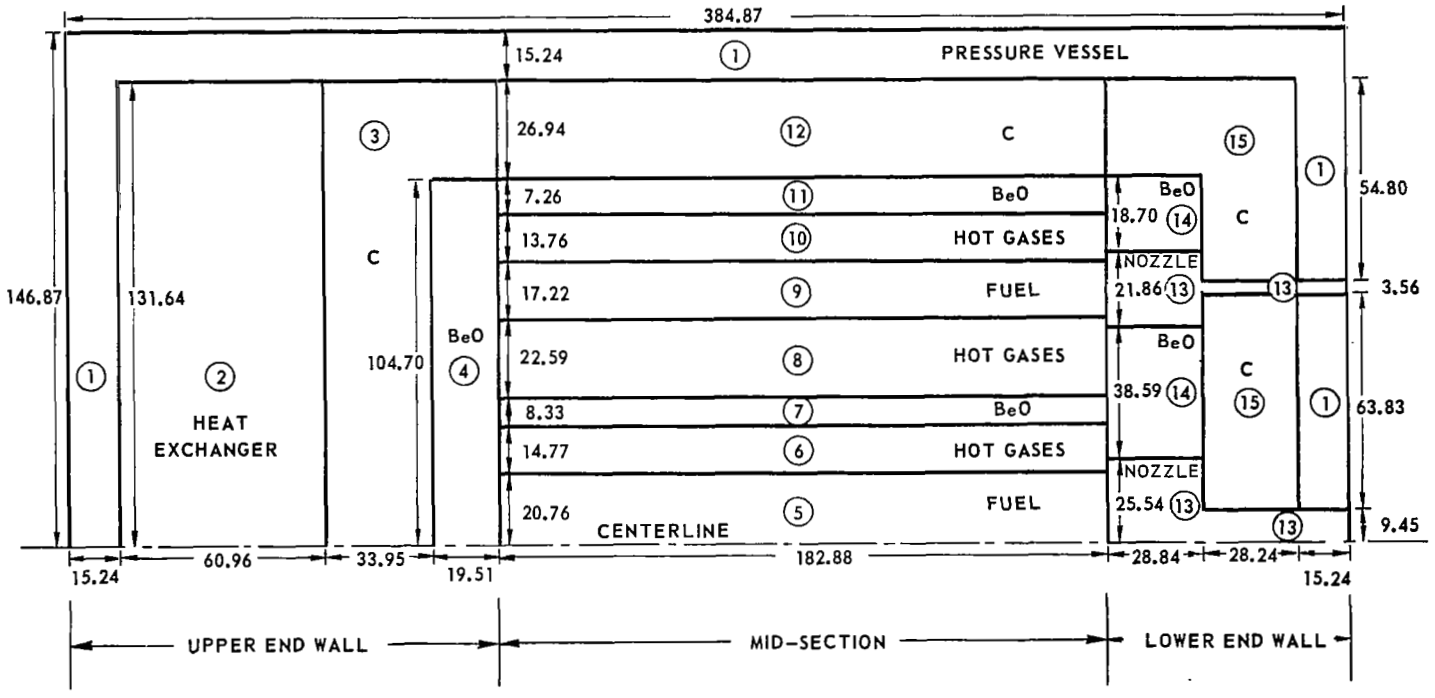

FIG. 3

FIG. 4

EFFECT OF TOTAL MODERATOR MASS ON U-233 CRITICAL MASS

REFERENCE ENGINE CONFIGURATION DESCRIBED IN FIG. 3 AND TABLES I AND II

RESULTS FROM 2-D DIFFUSION THEORY

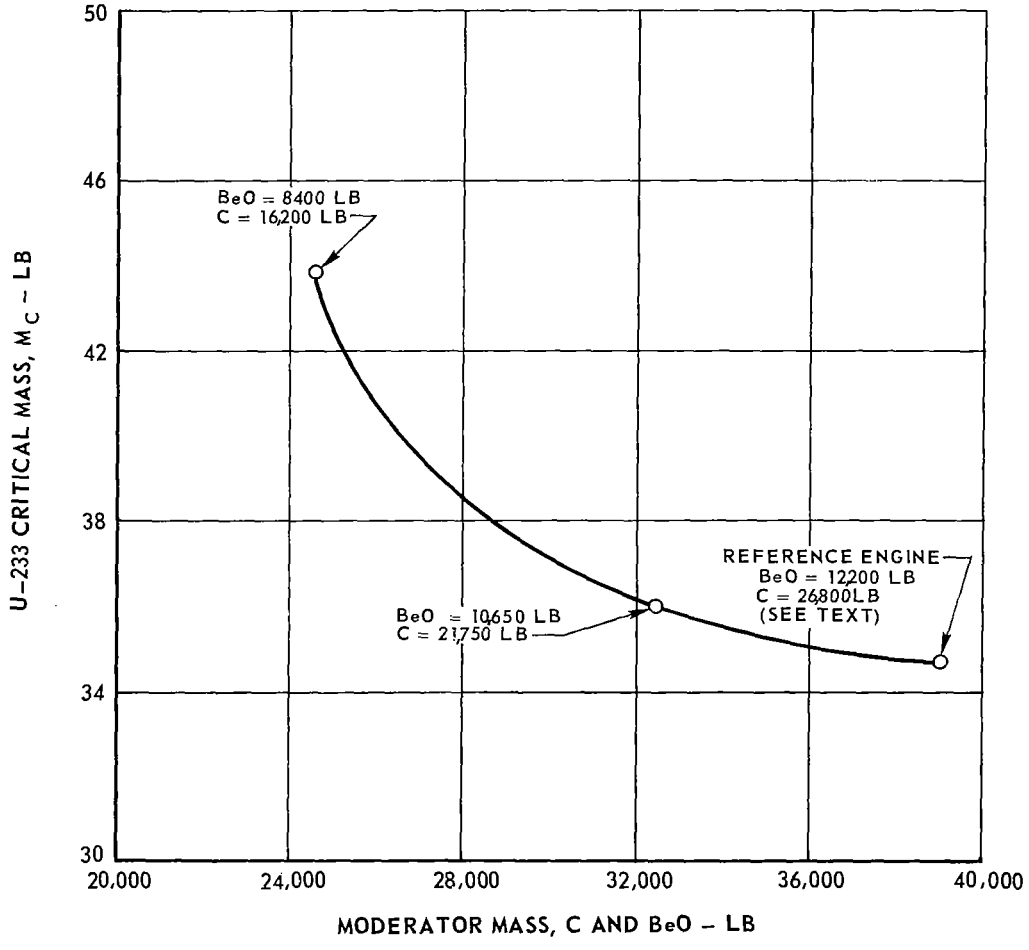

FIG. 5

EFFECT OF INTERNAL MODERATION ON U-233 CRITICAL MASS AND RATIO OF INNER--CAVITY TO OUTER-CAVITY POWER

RESULTS FROM 1-D, 4-GROUP TRANSPORT THEORY

1-D CONFIGURATION DESCRIBED IN FIG. 3 AND TABLE I; EFFECTIVE CYLINDER HEIGHT = 620 CM

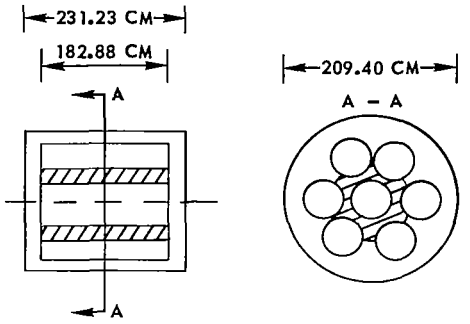

$$f_{IM} = \frac{\text{CROSS-HATCHED VOLUME}}{\text{TOTAL MODERATOR VOLUME}}$$

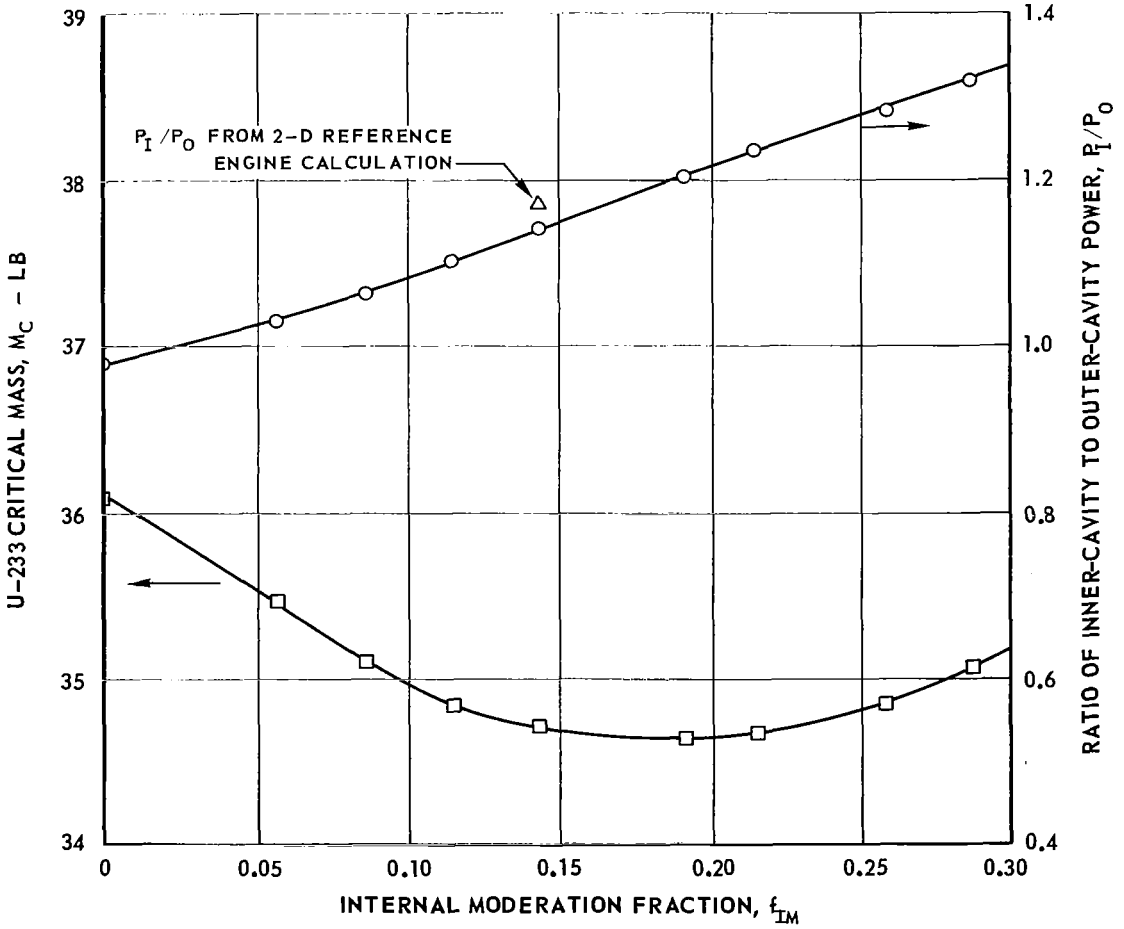

FIG. 6

EFFECT OF RATIO OF RADIAL – TO – TOTAL MODERATOR MASS ON U–233 CRITICAL MASS

REFERENCE ENGINE CONFIGURATION DESCRIBED IN FIG. 3 AND TABLES I AND II

RESULTS FROM 2–D DIFFUSION THEORY

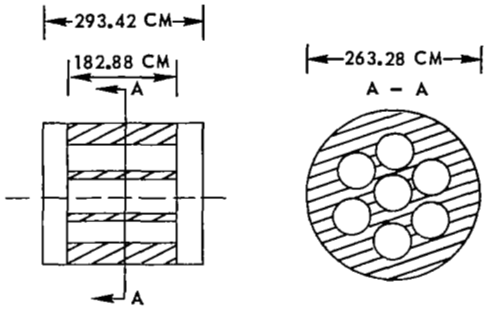

$$f_{RM} = \frac{\text{CROSS-HATCHED VOLUME}}{\text{TOTAL MODERATOR VOLUME}}$$

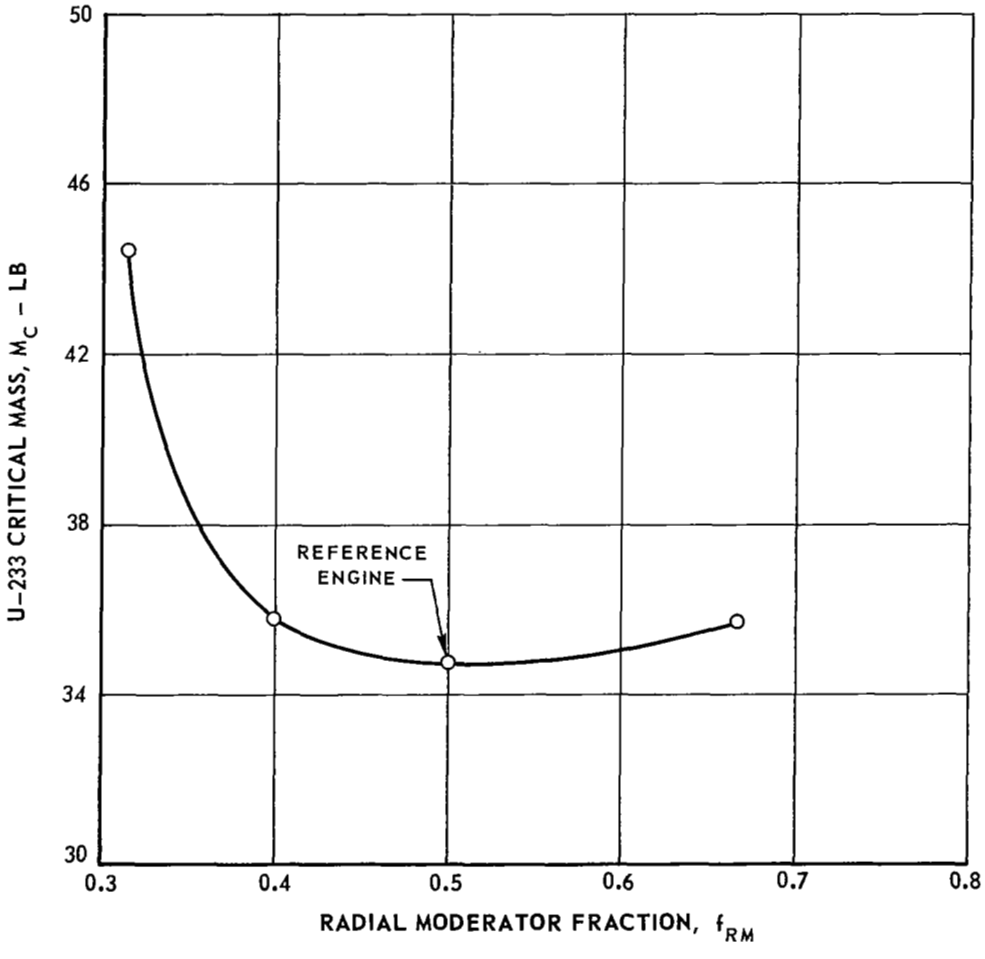

FIG. 7

EFFECT OF EFFECTIVE NOZZLE THROAT AREA ON U-233 CRITICAL MASS

REFERENCE ENGINE CONFIGURATION DESCRIBED IN FIG. 3 AND TABLES I AND II

RESULTS FROM 2-D DIFFUSION THEORY

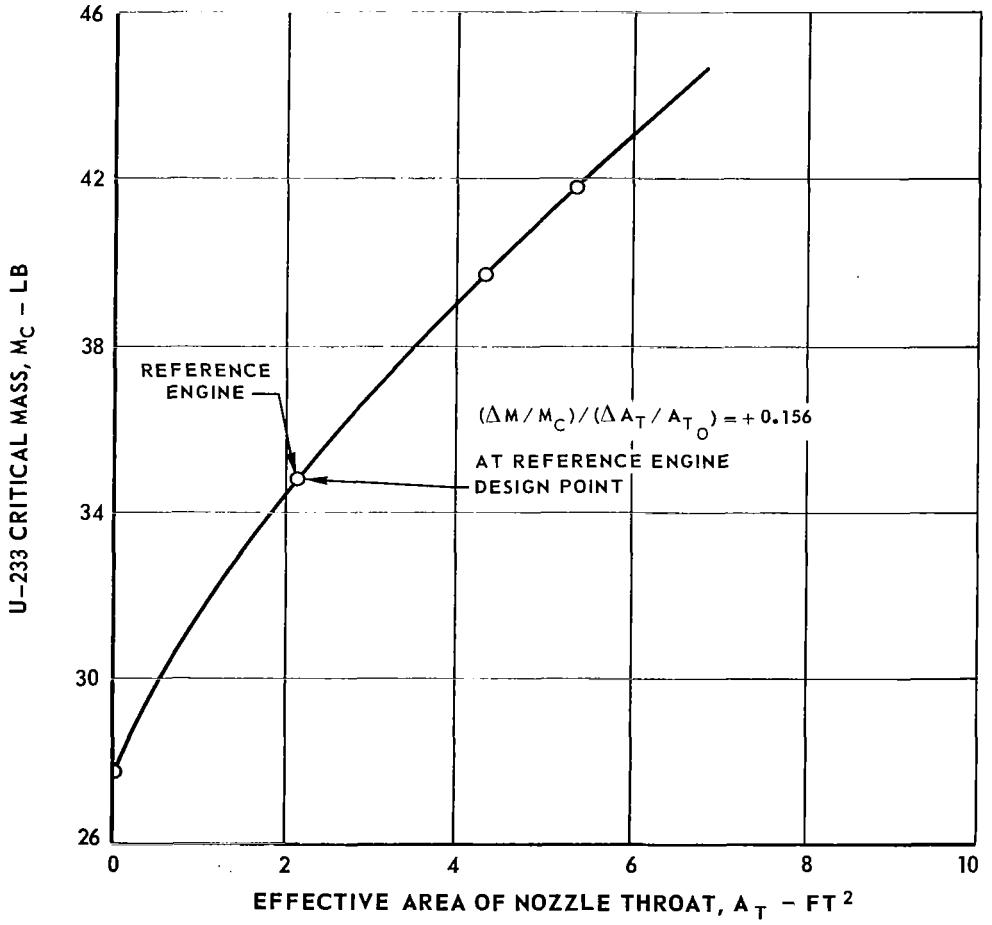

FIG. 8

EFFECT OF NOMINAL OPERATING TEMPERATURE ON THE EFFECTIVE MULTIPLICATION FACTOR

FUEL LOADING EQUAL TO 34.71 LB IN REFERENCE ENGINE

RESULTS FROM 1-D, 24-GROUP TRANSPORT THEORY; EFFECTIVE CYLINDER HEIGHT = 620 CM

THERMAL NEUTRON ENERGY LIMITS, 0.0 TO 8.32 ev

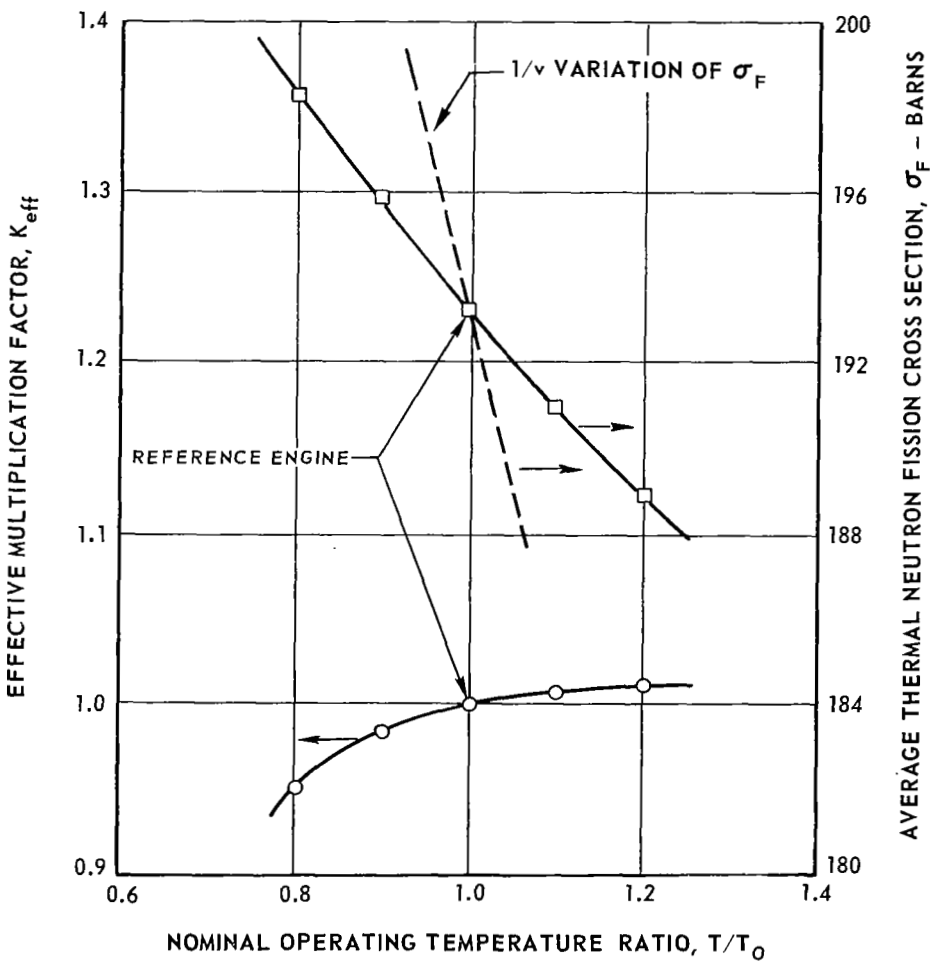

COMPARISON OF GROUP-4 RADIAL FLUX PLOTS FOR ONE- AND TWO-DIMENSIONAL NEUTRON DIFFUSION AND TRANSPORT THEORY CALCULATIONS

REFERENCE ENGINE CONFIGURATION DESCRIBED IN FIG. 3 AND TABLES I AND II
FLUXES CALCULATED AT AXIAL MID-PLANE AND NORMALIZED WITH RESPECT TO PEAK VALUE
GROUP-4 NEUTRON ENERGY LIMITS, 0.0 TO 8.32 ev

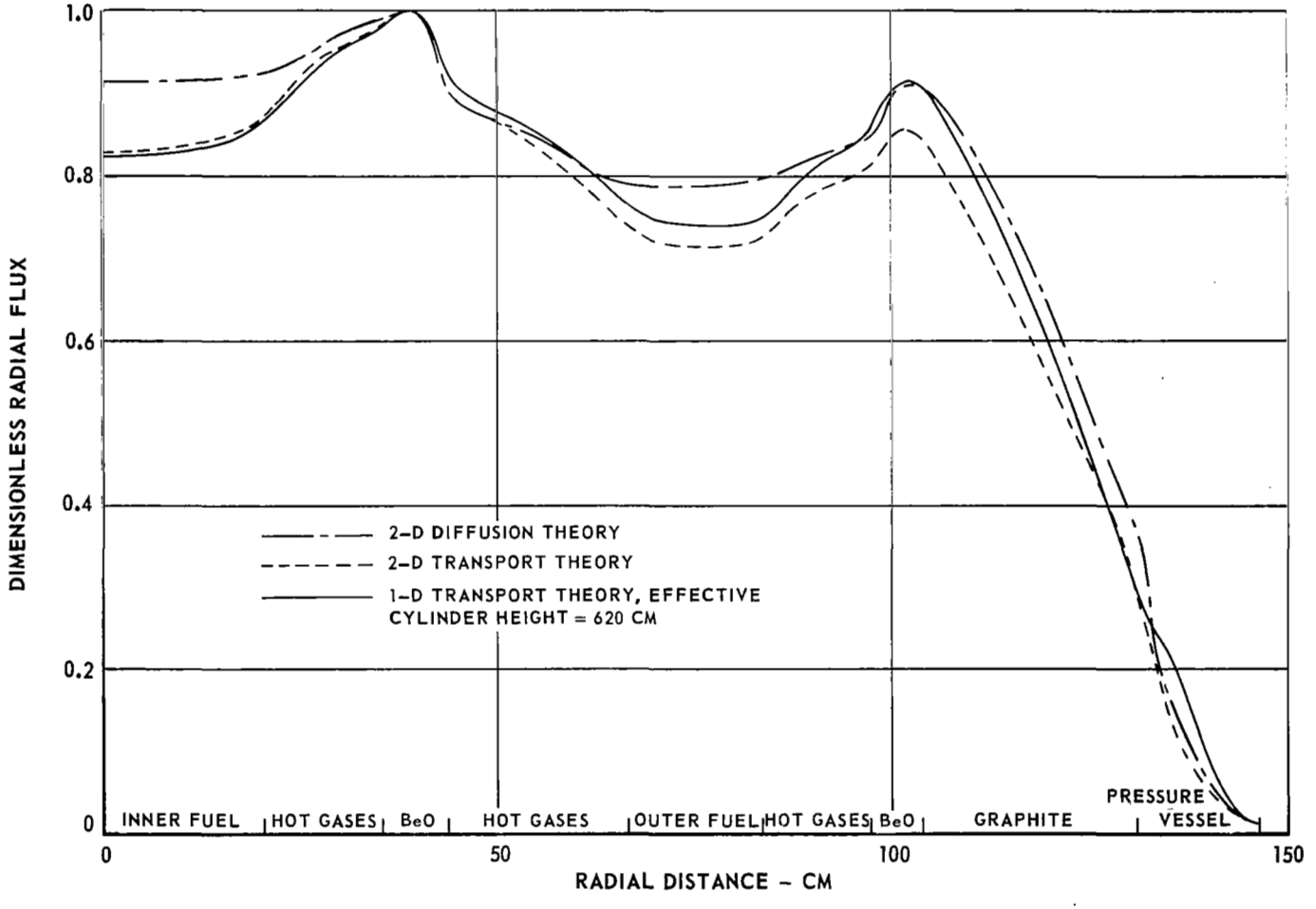

FIG. 9

FIG. 10

THERMAL NEUTRON FLUX SPECTRA IN SELECTED REGIONS OF NUCLEAR LIGHT BULB ENGINE

1-D CONFIGURATION DESCRIBED IN FIG. 3 AND TABLE I
RESULTS FROM 1-D, 24-GROUP TRANSPORT THEORY
FLUXES NORMALIZED SUCH THAT INTEGRATED FISSION NEUTRON SOURCE EQUALS 1 NEUTRON/SEC
ALL SPECTRA NORMALIZED WITH RESPECT TO PEAK VALUE

SPECTRA PEAK VALUES AND INTEGRATED NEUTRON FLUX		
REGION	PEAK VALUES NEUTRONS/CM^2 -SEC-ev	INTEGRATED FLUX 0.0 TO 8.32 ev NEUTRONS/CM^2 -SEC
PRESSURE VESSEL	0.01881	0.001622
GRAPHITE	0.01529	0.008499
OUTER FUEL	0.01960	0.01045
INNER BeO	0.03143	0.01378

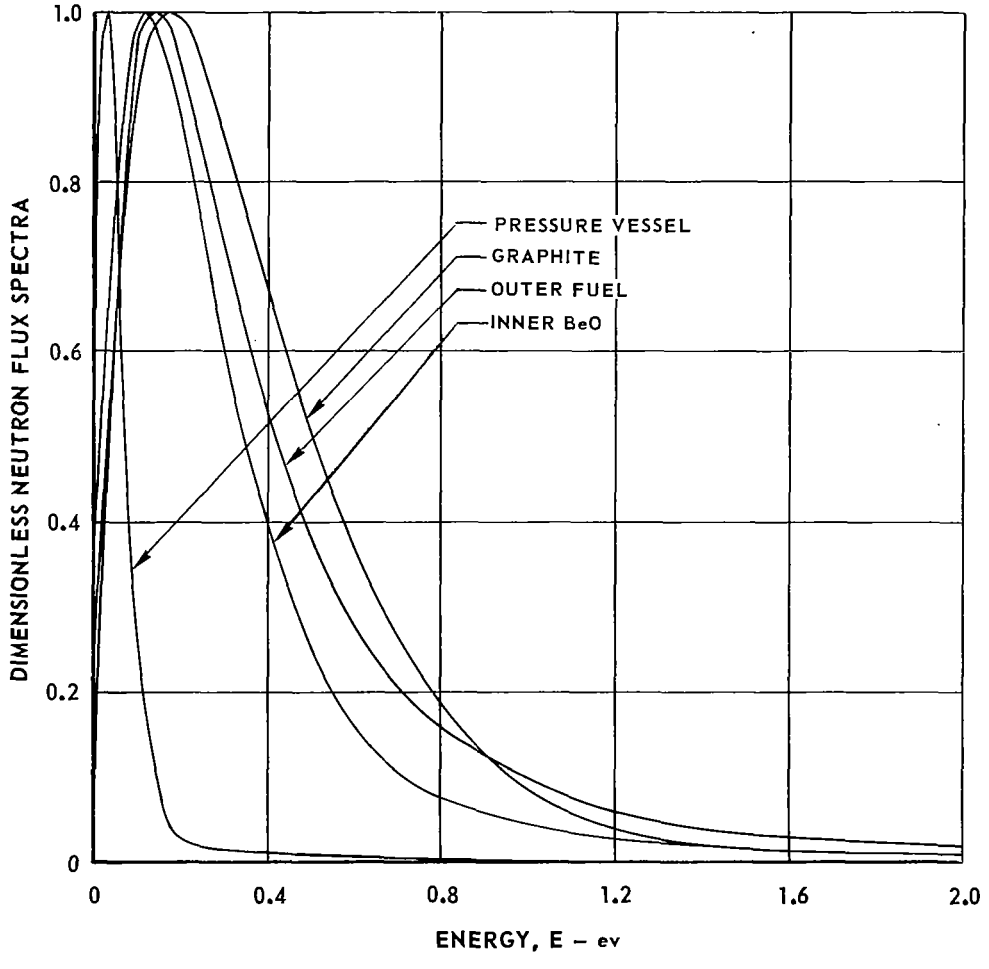

FIG. 11

NUCLEAR KINETIC EQUATIONS

a) NEUTRON LEVEL

$$\frac{d}{dt} n(t) = \frac{\delta k(t) - \beta}{\ell^*} n(t) + \sum_{i=1}^{6} \lambda_i C_i(t)$$

b) DELAYED NEUTRON PRECURSORS

$$\frac{d}{dt} C_i(t) = \frac{\beta_i}{\ell^*} n(t) - \left[\lambda_i + \lambda_F(t) \right] C_i(t)$$

c) NUCLEAR FUEL MASS

$$\frac{d}{dt} M(t) = \lambda_{F_0} M_0 - \lambda_F(t) M(t)$$

d) REACTIVITY FEEDBACK

$$\delta k(t) = \delta k_0 + 0.384 \frac{M(t) - M_0}{M_0}$$

e) STEADY-STATE REACTIVITY

$$\delta k_0 = \sum_{i=1}^{6} \frac{\beta_i \lambda_{F_0}}{\lambda_i + \lambda_{F_0}}$$

FIG. 12

VARIATION OF POWER LEVEL WITH STEP AND RAMP CHANGES IN REACTIVITY

U-233 FUEL

FUEL DECAY CONSTANT, $\lambda_{F_0} = 0.05\ SEC^{-1}$

REACTIVITY, $\delta k_0 = 0.00075 = \$0.30$

PROMPT NEUTRON LIFETIME, $\ell^* = 0.0005$ SEC

DELAYED NEUTRON FRACTION, $\beta = 0.0025$

a) RESPONSE TO STEP CHANGE IN REACTIVITY

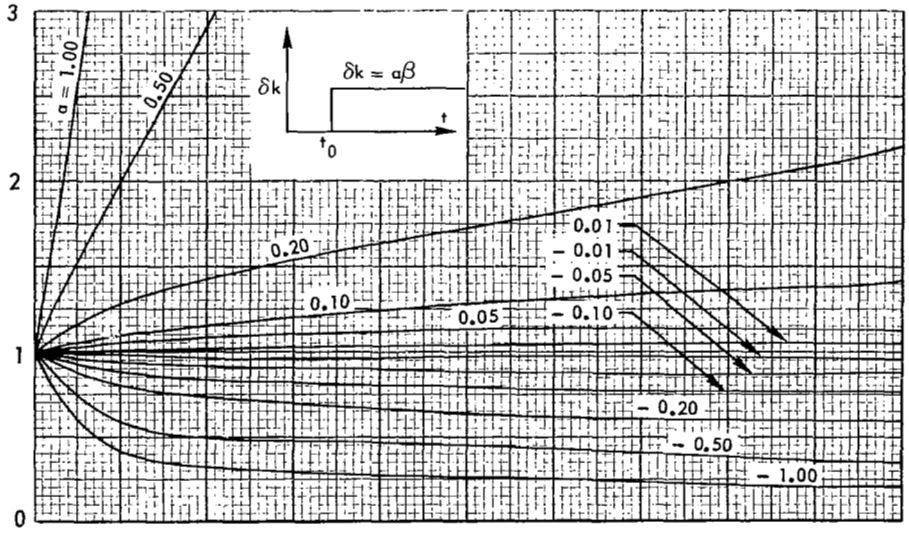

b) RESPONSE TO RAMP CHANGE IN REACTIVITY

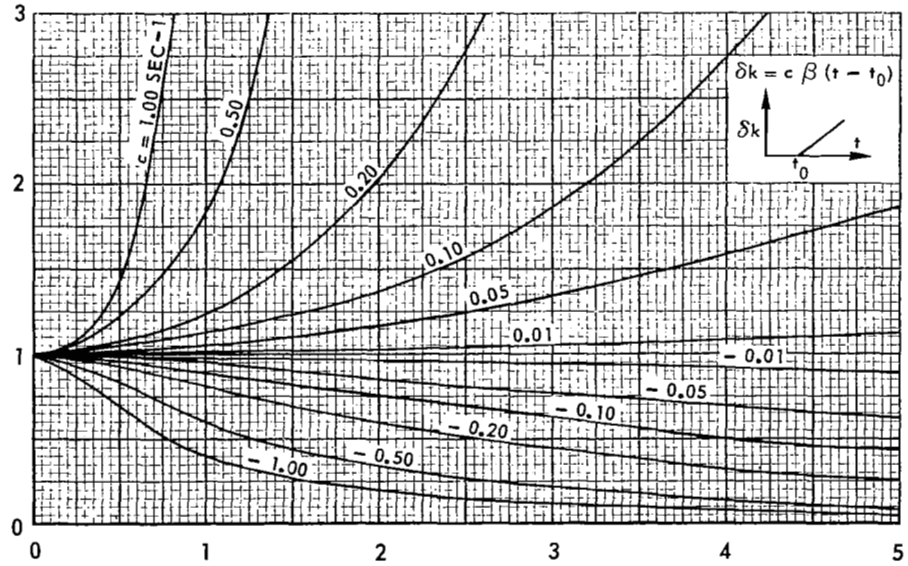

POWER LEVEL, $P/P_0 = n/n_0$

TIME AFTER REACTIVITY CHANGE, $(t - t_0)$ - SEC

FIG. 13

VARIATION OF POWER LEVEL WITH POSITIVE STEP AND RAMP CHANGES IN REACTIVITY FOR DIFFERENT VALUES OF FUEL DECAY CONSTANT

U–233 FUEL
PROMPT NEUTRON LIFETIME, $\ell^* = 0.0005$ SEC
DELAYED NEUTRON FRACTION, $\beta = 0.0025$

a) RESPONSE TO STEP CHANGE IN REACTIVITY

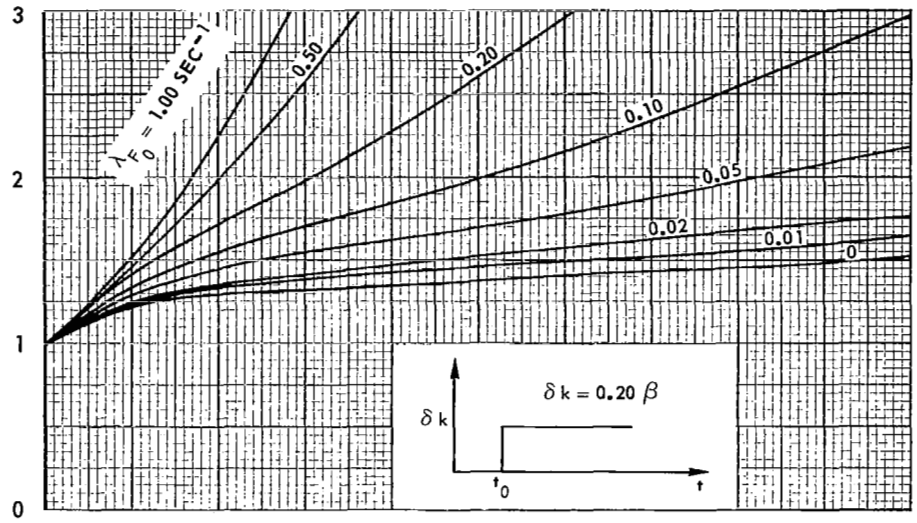

b) RESPONSE TO RAMP CHANGE IN REACTIVITY

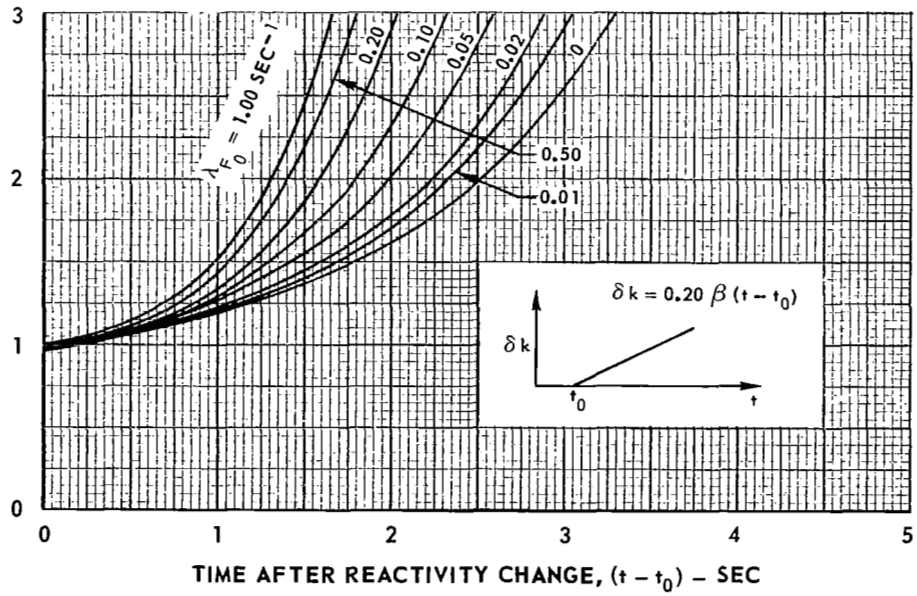

POWER LEVEL, $P/P_0 = n/n_0$

TIME AFTER REACTIVITY CHANGE, $(t - t_0)$ – SEC

FIG. 14

VARIATION OF POWER LEVEL WITH POSITIVE STEP AND RAMP CHANGES IN REACTIVITY FOR DIFFERENT VALUES OF PROMPT NEUTRON LIFETIME

U-233 FUEL

FUEL DECAY CONSTANT, $\lambda_{F_0} = 0.05\ SEC^{-1}$

DELAYED NEUTRON FRACTION, $\beta = 0.0025$

a) RESPONSE TO STEP CHANGE IN REACTIVITY

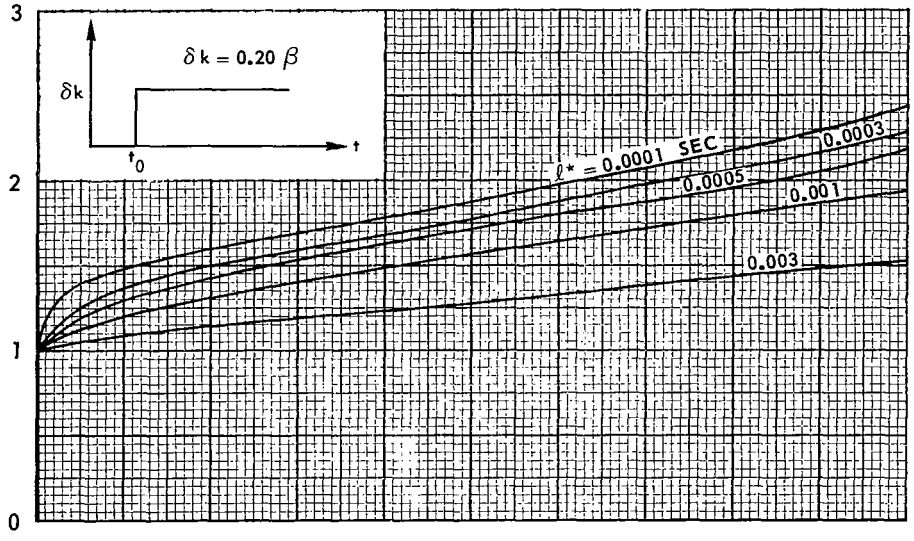

b) RESPONSE TO RAMP CHANGE IN REACTIVITY

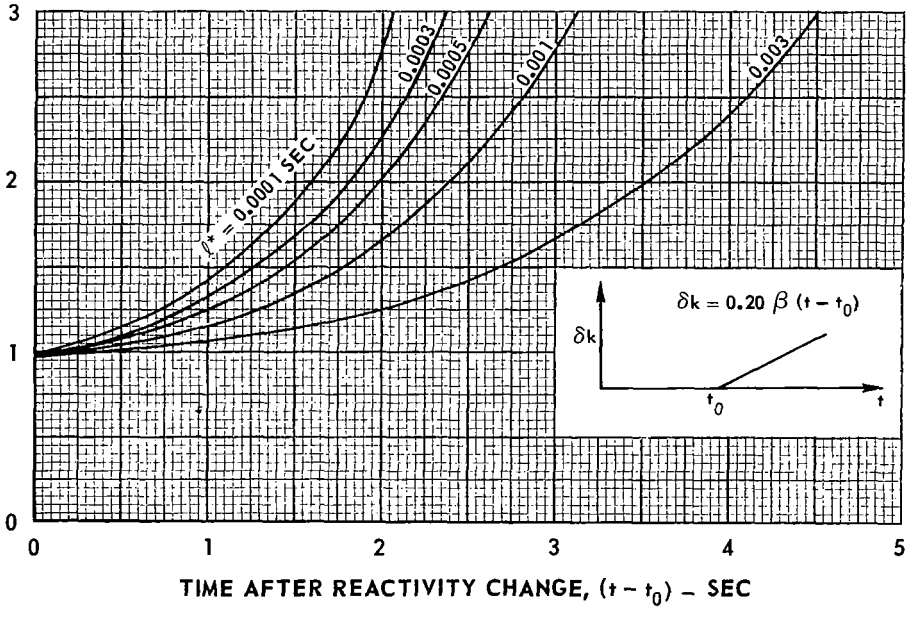

POWER LEVEL, $P/P_0 = n/n_0$

TIME AFTER REACTIVITY CHANGE, $(t - t_0)$ – SEC

FIG. 15

VARIATION OF FUEL LOADING WITH STEP CHANGES IN FUEL DECAY CONSTANT

U-233 FUEL

INITIAL FUEL MASS, $M_0 = 34.7$ LB

INITIAL FUEL DECAY CONSTANT, $\lambda_{F_0} = 0.05$ SEC^{-1}

a) RESPONSE TO NEGATIVE STEP CHANGE IN FUEL DECAY CONSTANT

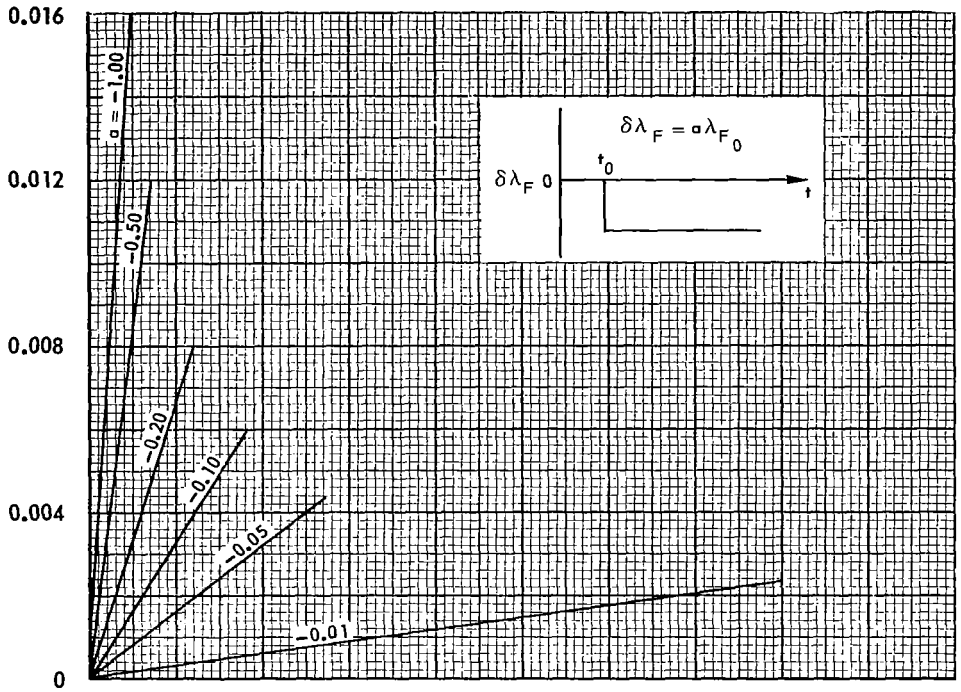

b) RESPONSE TO POSITIVE STEP CHANGE IN FUEL DECAY CONSTANT

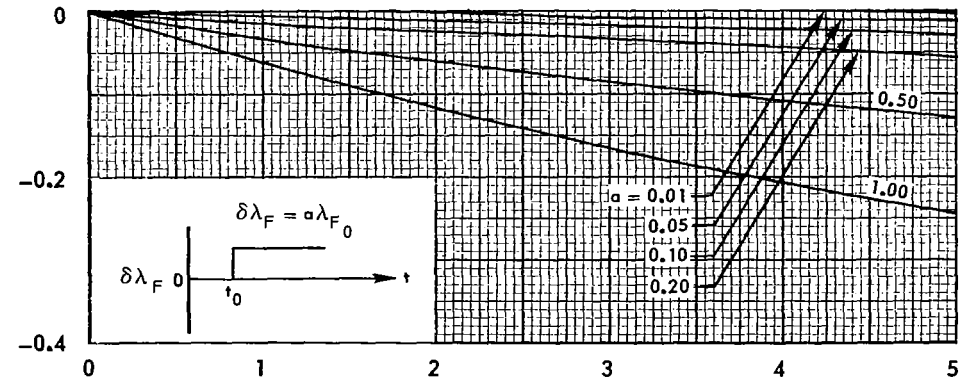

FRACTIONAL CHANGE IN FUEL LOADING, $\frac{M - M_0}{M_0}$

TIME AFTER FUEL DECAY CONSTANT CHANGE, $(t - t_0)$ – SEC

FIG. 16

VARIATION OF FUEL LOADING WITH RAMP CHANGES IN FUEL DECAY CONSTANT

U-233 FUEL
INITIAL FUEL MASS, $M_0 = 34.7$ LB
INITIAL FUEL DECAY CONSTANT, $\lambda_{F_0} = 0.05\ SEC^{-1}$

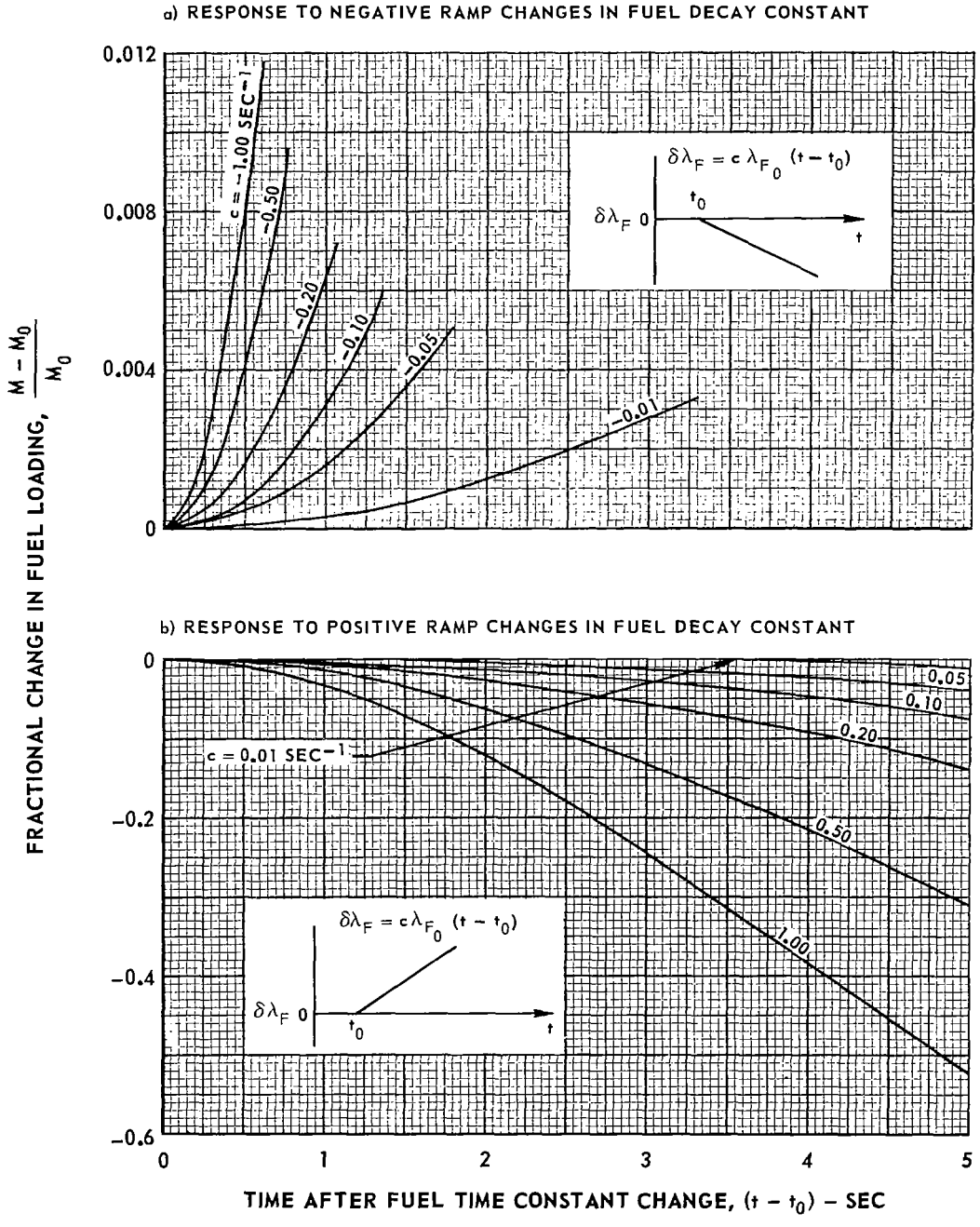

FIG. 17

VARIATION OF POWER LEVEL WITH STEP AND RAMP CHANGES IN FUEL DECAY CONSTANT

U-233 FUEL

INITIAL FUEL DECAY CONSTANT, $\lambda_{F_0} = 0.05\ SEC^{-1}$

INITIAL REACTIVITY, $\delta_{K_0} = 0.00075 = \$0.30$

PROMPT NEUTRON LIFETIME, $\ell^* = 0.0005$ SEC

DELAYED NEUTRON FRACTION, $\beta = 0.0025$

a) RESPONSE TO STEP CHANGE IN FUEL DECAY CONSTANT

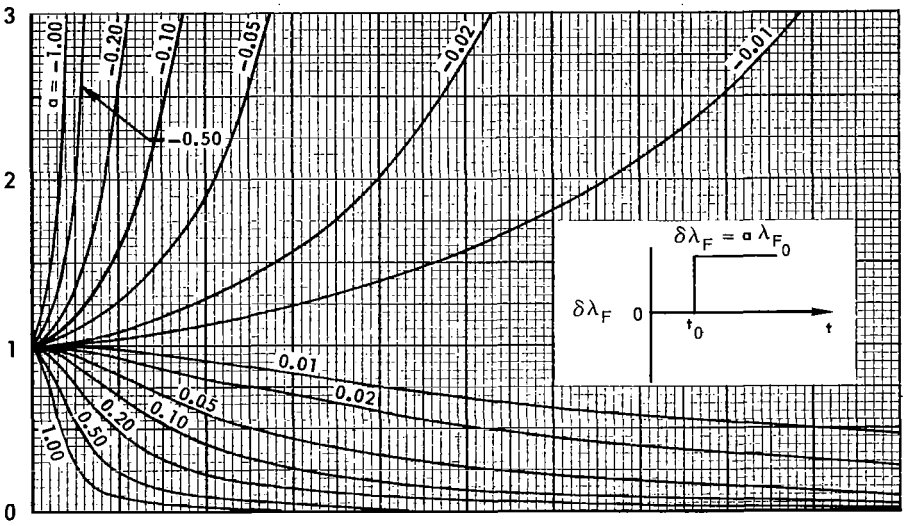

b) RESPONSE TO RAMP CHANGE IN FUEL DECAY CONSTANT

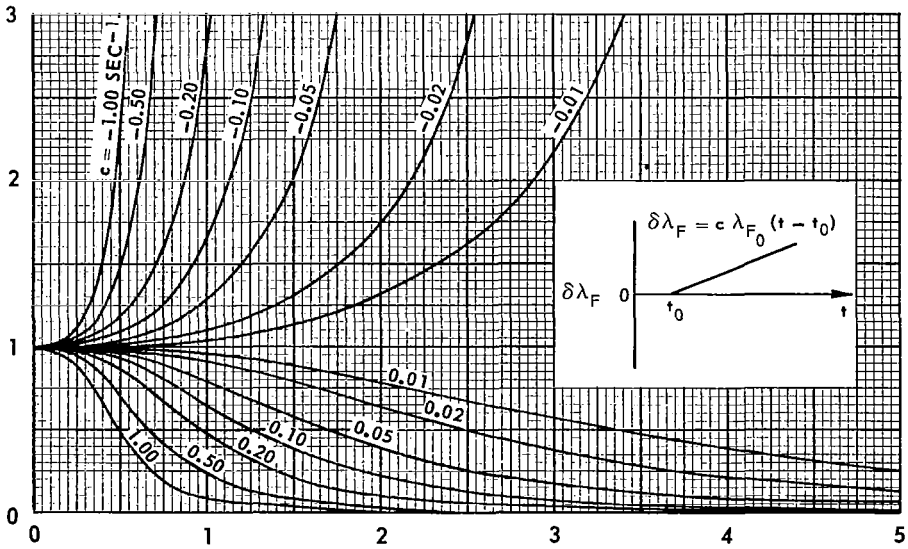

POWER LEVEL, $P/P_0 = n/n_0$

TIME AFTER FUEL TIME CONSTANT CHANGE, $(t - t_0)$ – SEC

FIG. 18

VARIATION OF FUEL LOADING WITH NEGATIVE RAMP CHANGES IN FUEL DECAY CONSTANT FOR DIFFERENT INITIAL VALUES OF FUEL DECAY CONSTANT

U-233 FUEL

INITIAL FUEL MASS, $M_0 = 34.7$ LB

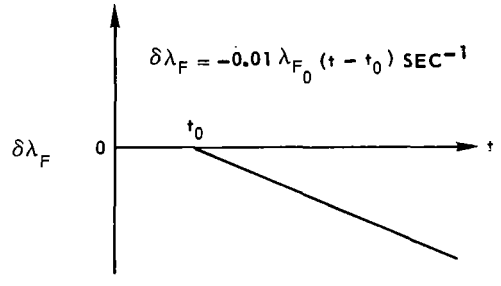

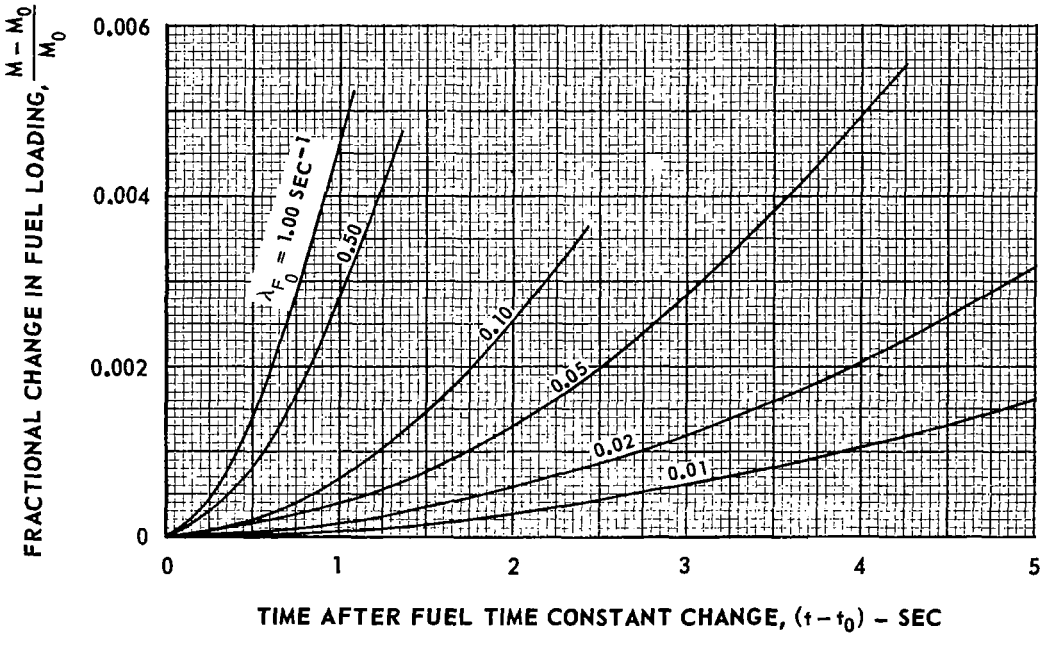

FIG. 19

VARIATION OF POWER LEVEL WITH NEGATIVE RAMP CHANGES IN FUEL DECAY CONSTANT FOR DIFFERENT PROMPT NEUTRON LIFETIMES AND FOR DIFFERENT INITIAL VALUES OF FUEL DECAY CONSTANT

U-233 FUEL

DELAYED NEUTRON FRACTION, $\beta = 0.0025$

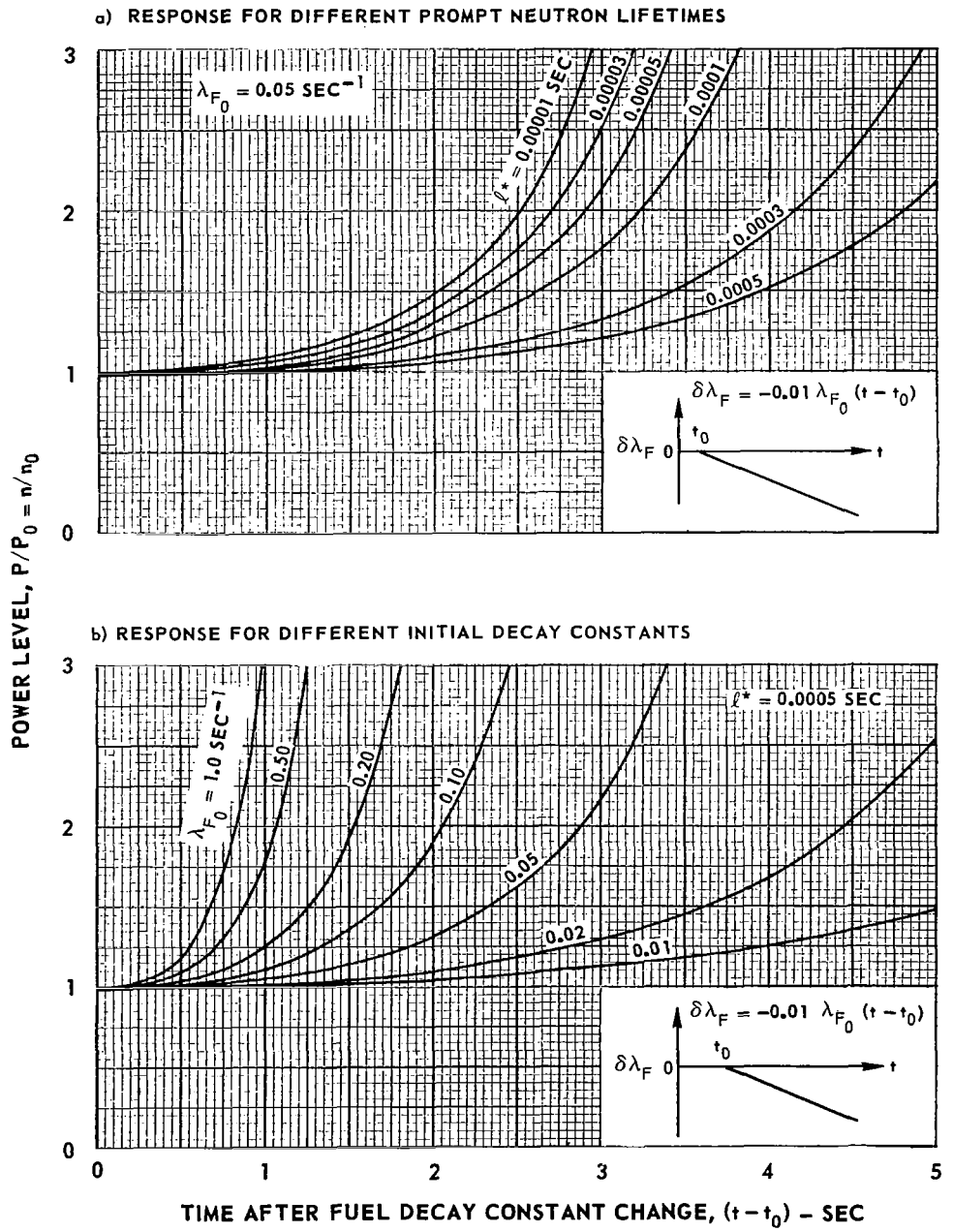

GAIN AND PHASE DIAGRAMS FOR RESPONSE OF NEUTRON LEVEL TO SMALL SINUSOIDAL OSCILLATIONS IN REACTIVITY

U-233 FUEL

PROMPT NEUTRON LIFETIME, $\ell^* = 0.0005$ SEC

DELAYED NEUTRON FRACTION, $\beta = 0.0025$

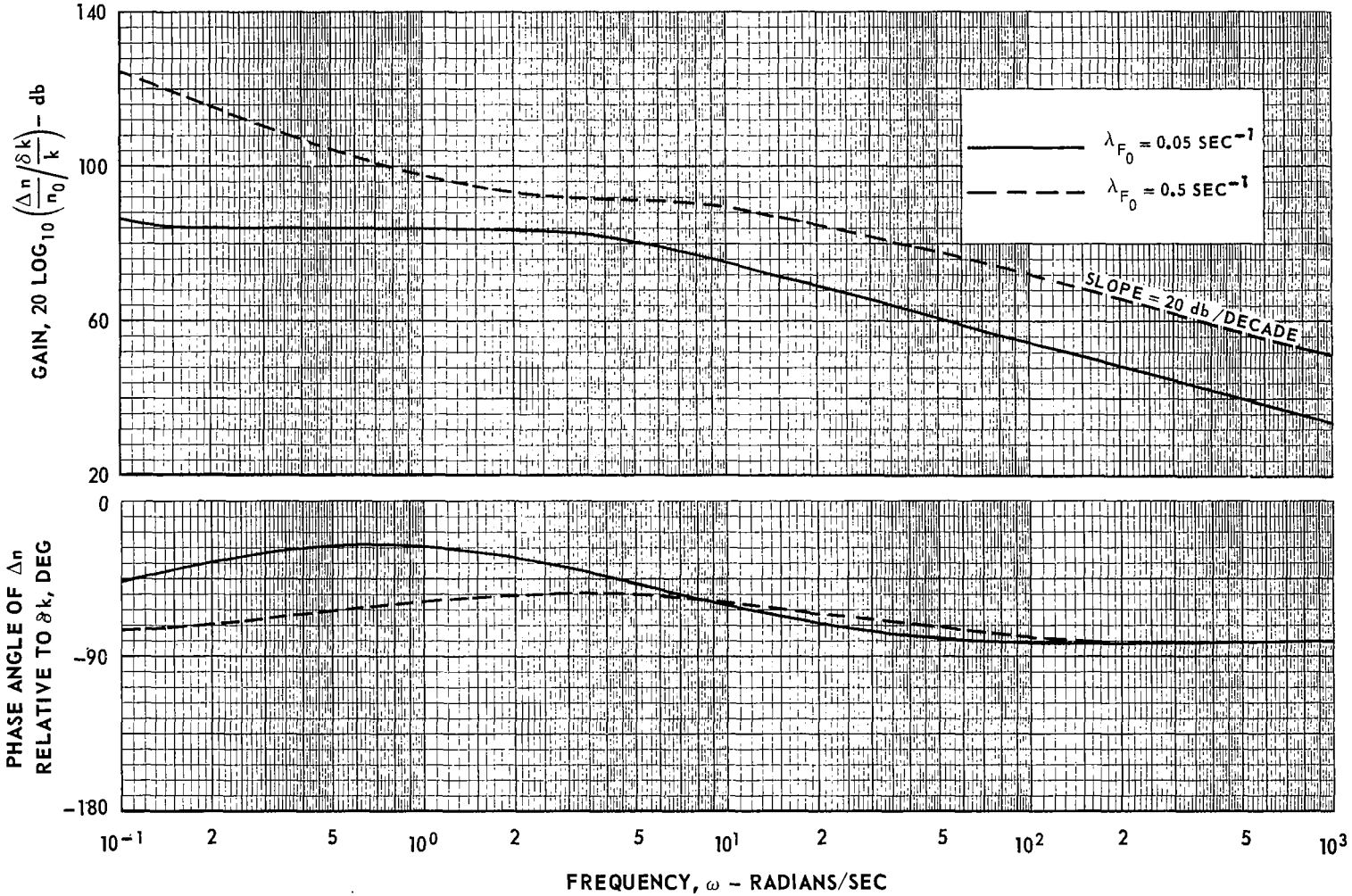

FIG. 20

GAIN AND PHASE DIAGRAMS FOR RESPONSE OF NEUTRON LEVEL TO SMALL SINUSOIDAL OSCILLATIONS IN FUEL DECAY CONSTANT

U-233 FUEL

PROMPT NEUTRON LIFETIME, $\ell^* = 0.0005$ SEC

DELAYED NEUTRON FRACTION, $\beta = 0.0025$

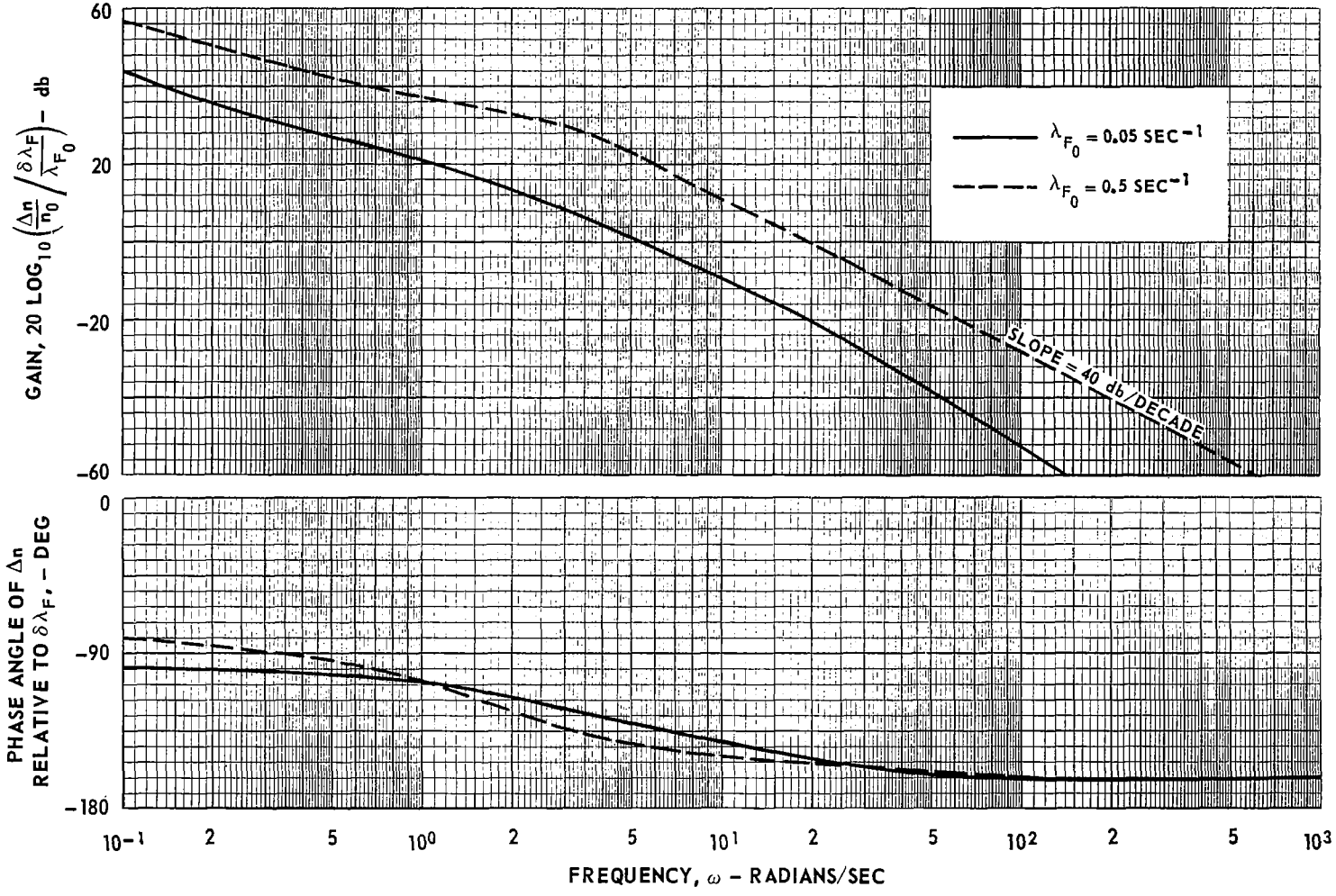

FIG. 21

FIG. 22

ENERGY RELEASED BY NEUTRONS, GAMMA RAYS, BETA PARTICLES, AND FISSION FRAGMENTS AS A FUNCTION OF TIME AFTER FISSION OF U-233

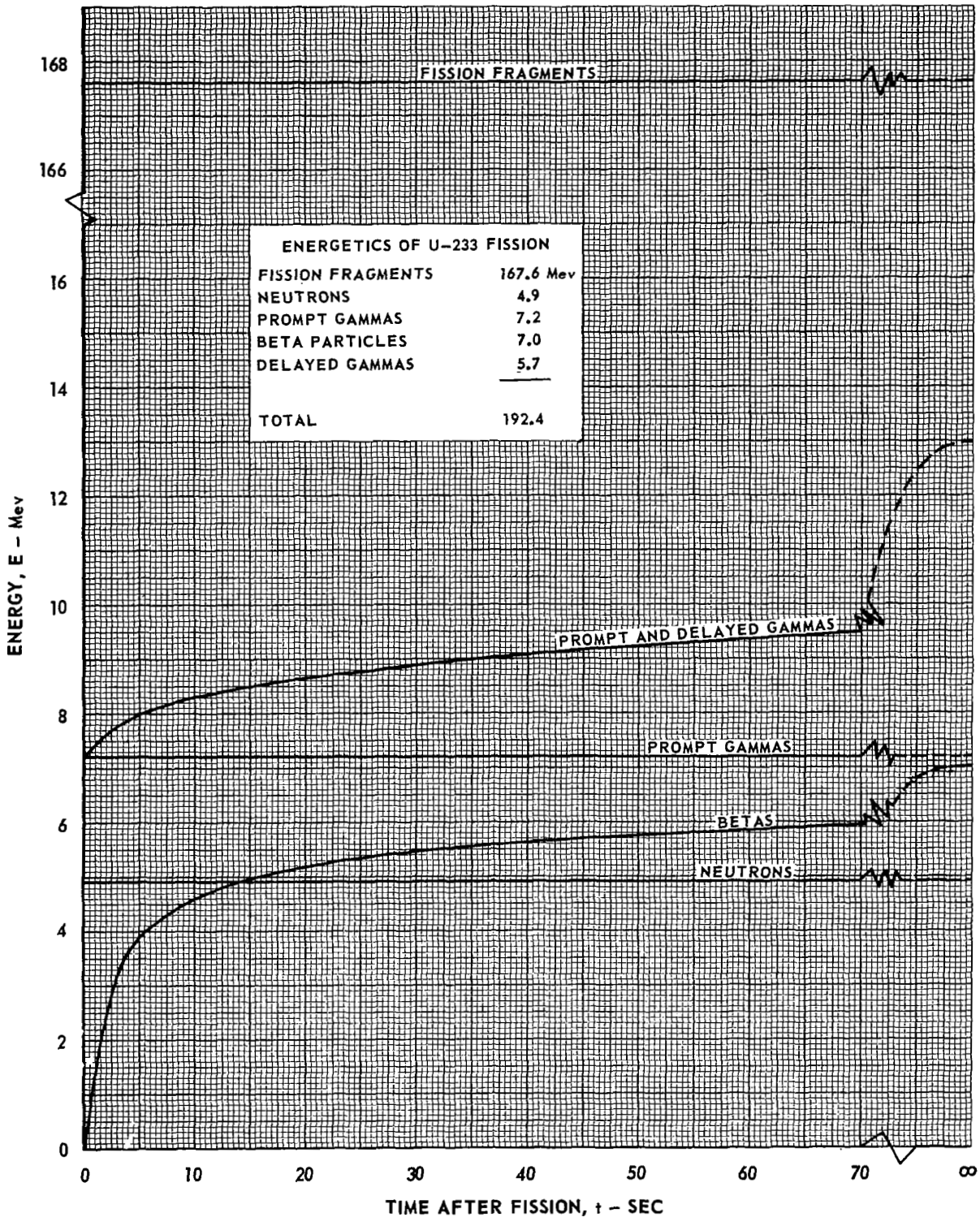

NASA-Langley, 1969 — 25 CR-1315